



TALLINN UNIVERSITY OF TECHNOLOGY
SCHOOL OF ENGINEERING
Mechatronics and Autonomous Systems Centre

COST EFFECTIVE WIDE AREA CITY ENVIRONMENTAL MONITORING

TASUV LAIAS PIIRKONNAS PAIKNEV KESKKONNASEIRE

MASTER THESIS

Üliõpilane: Tomisin Anthony Abimbola
/nimi/

Üliõpilaskood: 184510MAHM
Dmitry Shvarts

Juhendaja: Jurgo Preden

Tallinn 2020

(On the reverse side of title page)

AUTHOR'S DECLARATION

Hereby I declare, that I have written this thesis independently.

No academic degree has been applied for based on this material. All works, major viewpoints and data of the other authors used in this thesis have been referenced.

"24" May 2020

Author:

/signature /

Thesis is in accordance with terms and requirements

"....." 20....

Supervisor:

/signature/

Accepted for defence

".....".....20... .

Chairman of theses defence commission:

/name and signature/

Non-exclusive Licence for Publication and Reproduction of Graduation Thesis¹

I, Tomisin Anthony Abimbola (name of the author) (date of birth: 26-09-1990) hereby

1. grant Tallinn University of Technology (TalTech) a non-exclusive license for my thesis Cost Effective Wide Area City Environmental Monitoring System,
(*title of the graduation thesis*)

supervised by Jurgo Preden and Dmitry Shvarts,

(*Supervisor's name*)

1.1 reproduced for the purposes of preservation and electronic publication, incl. to be entered in the digital collection of TalTech library until expiry of the term of copyright;

1.2 published via the web of TalTech, incl. to be entered in the digital collection of TalTech library until expiry of the term of copyright.

1.3 I am aware that the author also retains the rights specified in clause 1 of this license.

2. I confirm that granting the non-exclusive license does not infringe third persons' intellectual property rights, the rights arising from the Personal Data Protection Act or rights arising from other legislation.

¹ *Non-exclusive Licence for Publication and Reproduction of Graduation Thesis is not valid during the validity period of restriction on access, except the university's right to reproduce the thesis only for preservation purposes.*

_____ (*signature*)

_____ (*date*)

Mechatronics and Autonomous System

THESIS TASK

Student: Tomisin Anthony Abimbola, 184510MAHM (name, student code)

Study programme: MAHM02/18 - Mechatronics (code and title)

main specialty: Mechatronics

Supervisor(s): Dmitry Shvarts, Research Scientist (position, name, phone)

Consultants: Jurgo Preden, CEO, Thinnect OÜ (name, position)

..... (company, phone, e-mail)

Thesis topic:

(in English) Cost Effective Wide Area City Environmental Monitoring

(in Estonian) Tasuv laias piirkonnas paiknev keskkonnaseire

Thesis main objectives:

1. To calibrate the multi-gas sensor used in the sensor nodes of the Environmental monitoring system prototype.
2. To write the driver for the Multi Gas sensor unit in order to acquire data and process it to conform with engineering standards.
3. To analyze the data collected by the existing sensor nodes and validate with the conventional systems.
4. Recommend a power management strategy to improve the energy efficiency of the system.

Thesis tasks and time schedule:

No	Task description	Deadline
1.	Planning and review of system hardware and datasheets	February 2020
2.	Sensor calibration and design of sensor firmware algorithm	March 2020
3.	Sensor data analysis and presentation of results	April 2020
4.	Drawing conclusion and recommendation of energy efficiency optimization.	May 2020

Language: English **Deadline for submission of thesis:** "25" May 2020.

Student: Tomisin Anthony Abimbola "22" May 2020

/signature/

Supervisor: Dmitry Shvarts "22" May 2020

/signature/

Consultant: Jurgo Preden "22" May 2020

/signature/

Head of study programme: Mart Tamre "22" May 2020

/signature/

Terms of thesis closed defence and/or restricted access conditions to be formulated on the reverse side

CONTENTS

PREFACE	8
List of abbreviations and symbols	9
List of figures.....	11
List of tables.....	14
1. INTRODUCTION.....	15
1.1 Problem statement	16
1.2 Chapters review	18
2. STATE OF THE ART	19
2.1 Air pollution monitoring systems.....	19
2.2 Gas sensors	20
2.2.1 Solid-state Gas Sensor	21
2.3 Particulate Matter Sensor.....	22
2.4 Wireless sensor network.....	23
3. METHODOLOGY AND DEVICE DEVELOPMENT	27
3.1 General overview of the environmental monitoring system	27
3.2 Hardware Architecture.....	28
3.2.1 Silabs Mighty Gecko 32-bit SoC	28
3.2.2 PMS7003 Particle Concentration Sensor	30
3.2.3 MICS-6814 Multi gas sensor	32
3.2.4 BME280 Digital Humidity, Pressure and Temperature sensor	36
3.2.5 Thinnect Smart City Gateway (TSCG)	38
3.2 Software Design	40
3.2.1 General overview of software architecture	40
3.2.2 Data acquisition from sensors and transmission	41
4. RESULTS	43
4.1 Calibrating the MICS-6814 Multi Gas Sensor	43
4.1.1 Deriving the relationship between ADC digital output value and sensor resistance.....	44

4.1.2	Deriving the base sensing resistance in air (R_o)	45
4.1.3	Deriving the relationship between sensor resistance ratio (R_s/R_o) and the gas concentration in PPM	46
4.2	Firmware development for the Multi Gas Sensor	49
4.3	Analysis of Data collected by sensor nodes and validation.....	50
4.3.1	Overview of system implementation	50
4.3.2	Data analysis and validation of Thinnect’s sensor node around Liivalaia station	51
4.4	Energy efficiency recommendation.....	60
5.	SUMMARY.....	63
5.1	Conclusion	63
5.2	Kokkuvõte eesti keeles.....	65
5.3	Future Work.....	67
	LIST OF REFERENCES	68
	APPENDIX 1 Plots showing sensor data obtained on 30-04-2020 from the Thinnect node located at Rahu, Tallinn	74
	APPENDIX 2 Firmware code for the multi gas sensor.....	76
	APPENDIX 3 The sensor node energy consumption and efficiency analysis	79
	APPENDIX 4 Pictures showing the Thinnect sensor node for environmental monitoring.....	80

PREFACE

My sincere appreciation goes to God; the giver of knowledge for giving me the privilege to complete this research work successfully.

I wish to express my deepest gratitude to my supervisor; The CEO of Thinnect OU (Jurgo Preden) for granting me the opportunity, support and contributing to this impactful project, aimed at solving a problem in the city of Tallinn. To other staffs of Thinnect, Raido, Joss and Konstantin, I say a big thank you. To my co-supervisor, Dmitry Shvarts thank you for your contributions and support towards the completion of this research work.

My special gratitude also goes to my parents Mr. and Mrs. Abimbola, siblings Femi, Bukunmi and Gbenga Abimbola for their continual prayer, support and love over the years. To my Fiancée, Deborah, I would like to use this medium to say I appreciate all your prayers, love and words of encouragement. You've been a great source of inspiration to me.

And finally, Young Olutosin my special friend whom I met during the course of this Master program, I am indebted to you for your motivation and immense support from the beginning of this journey till this final stage.

Thank you all for your support, contributions and assistance at different capacities. They formed a milestone in the completion of this research project.

This research work is an industry-based initiative done in collaboration with Thinnect OU. It is aimed at improving the functionality and efficiency of the environmental monitoring sensor node developed in the Smart Environment Networking Technologies (SMENETE) project, a cost-effective environmental monitoring system (EMS) suitable for wide area use in a smart city, like Tallinn.

Keywords- environmental monitoring system, air pollution monitoring, smart environment, gas sensor calibration, master thesis

List of abbreviations and symbols

ADC	Analog-to-Digital Converter
API	Application Programming Interface
BLE	Bluetooth Low Energy
CO	Carbon Monoxide
CSN	Community Sensor Network
I2C	Integrated to Integrated Circuit
IDE	Integrated Development Environment
MCU	Microcontroller Unit
MEMS	Micro Electro Mechanical Systems
NH ₃	Ammonia
NO ₂	Nitrogen Dioxide
OPC	Optical Particle Counter
PCB	Printed Circuit Board
PM	Particulate Matter
PM ₁	Particulate matter less than 1 micrometres
PM _{2.5}	Particulate matter less than 2.5 micrometres
PM ₁₀	Particulate matter less than 10 micrometres
PM ₁	Particulate matter less than 1 micrometres
PPM	Parts Per Million
RH	Relative Humidity
R _o	Base Sensing Resistance in Air
R _s	Current Sensing Resistance in Air
SCK	Serial Clock
SCL	Serial Clock Line
SDA	Serial Data Line
SDI	Serial Data Input
SDO	Serial Data Output
SMENETE	Smart Environment Networking Technologies
SMO	Semiconductor Metal Oxide
SoC	System on Chip
SPI	Serial Peripheral Interface
SSN	Static Sensor Network
TSCG	Thinect Smart City Gateway
UART	Universal Asynchronous Receiver and Transceiver
VOC	Volatile Organic Compounds

VSN	Vehicle Sensor Network
WHO	World Health Organization
WSN	Wireless Sensor Network

List of figures

Figure 2.1 A bead-type solid-state gas sensor [36].....	21
Figure 2.2 A chip-type solid-state gas sensor [36].....	22
Figure 2.3 Typical architecture of a WSN [39].....	24
Figure 3.1 The architecture of the Environmental Monitoring System.....	27
Figure 3.2 The architecture of the EFR32MG SoC [63].....	29
Figure 3.3 Functional block diagram of the PMS7003 particle sensor [64].....	30
Figure 3.4 Functional block diagram of the PMS7003 particle sensor [64].....	31
Figure 3.5 The implementation architecture of the particle sensor on PCB [70].....	31
Figure 3.6 The MICS-6814 multi gas sensor power supply circuit recommended by the manufacturer [66].....	33
Figure 3.7 The implementation of the The MICS-6814 multi gas sensor power supply on PCB [65].....	34
Figure 3.8 The schematic showing how the ADC chip was interfaced with the MICS-6814 multi-gas sensor [65].....	35
Figure 3.9 The relationship between the concentration of gas in PPM and the ratio of current sensor resistance (R_s) to base sensing resistance in synthetic air (R_o) for oxidation sensor [66].....	36
Figure 3.10 The relationship between the concentration of gas in PPM and the ratio of current sensor resistance (R_s) to base sensing resistance in synthetic air (R_o) for oxidation sensor (NO_2) [66].....	36
Figure 3.11 The block diagram of the BME280 humidity, pressure and temperature sensor [67].....	37
Figure 3.12 The schematic showing how the BME280 humidity, pressure and temperature sensor was integrated on the PCB [65].....	37
Figure 3.13 The software architecture of the environmental monitoring system.....	40
Figure 4.1 The circuit diagram for determining the sensing resistance of MICS-6814 multi gas sensor.....	44
Figure 4.2 A plot showing the relationship between PPM and sensor resistance ratio (R_s/R_o) for CO.....	47
Figure 4.3 A plot showing the relationship between PPM and sensor resistance ratio (R_s/R_o) for NO_2	47
Figure 4.4 A plot showing the relationship between PPM and sensor resistance ratio (R_s/R_o) for NH_3	47
Figure 4.5 Environmental monitoring system prototype.....	50
Figure 4.6 A plot showing the temperature reading on 30-April-2020 obtained from the Thinnect sensor node located in Liivalaia, Tallinn.....	51

Figure 4.7 A plot showing the atmospheric pressure reading on 30-April-2020 obtained from the Thinnect sensor node located in Liivalaia, Tallinn.....52

Figure 4.8 A plot showing the relative humidity reading on 30-April-2020 obtained from the Thinnect sensor node located in Liivalaia, Tallinn.....53

Figure 4.9 A plot showing the Particulate Matters reading on 30-April-2020 obtained from the Thinnect sensor node located in Liivalaia, Tallinn chart for 30-April-2020.....54

Figure 4.10 A plot showing fine Particulate Matter (PM10) chart for 30-April-2020 from the conventional environmental monitoring station located in Liivalaia, Tallinn [70]..... 54

Figure 4.11 Two plots showing carbon monoxide level on 30-April-2020 obtained from the Thinnect sensor node versus the conventional air monitoring station located in Liivalaia, Tallinn.....55

Figure 4.12 A side-by-side comparison of charts showing carbon monoxide level on 30-April-2020 obtained from the Thinnect sensor node (using the experimental calibration constant, $R_o=12.5k\Omega$) versus the conventional air monitoring station (right chart) located in Liivalaia, Tallinn.....56

Figure 4.13 A side-by-side comparison of charts showing nitrogen dioxide level on 30-April-2020 obtained from the Thinnect sensor node (left chart) versus the conventional air monitoring station (right chart) located in Liivalaia, Tallinn.....57

Figure 4.14 Side by side comparison of the nitrogen dioxide level on 06-May-2020 obtained from the standalone sensor node (mg/m^3) versus the conventional air monitoring station ($\mu g/m^3$) located in Liivalaia, Tallinn.....58

Figure 4.15 A chart showing the current total energy consumption of the Thinnect sensor node watt-hours/day (red) versus the estimated total energy consumption in watt-hours/day (blue) if this recommendation is implemented.....61

Figure 4.16 State representation of energy efficiency recommendation.....62

Figure A1.1 A side-by-side comparison of charts showing carbon monoxide level on 30-April-2020 obtained from the Thinnect sensor node (using the experimental calibration constant, $R_o=12.5k\Omega$) versus the conventional air monitoring station (right chart) located in Rahu, Tallinn.....74

Figure A1.2 A side-by-side comparison of charts showing nitrogen dioxide level on 30-April-2020 obtained from the Thinnect sensor node (in mg/m^3) versus the conventional air monitoring station (in $\mu g/m^3$) located in Rahu, Tallinn.....74

Figure A1.3 A plot showing the temperature reading on 30-April-2020 obtained from the Thinnect sensor node located in Rahu, Tallinn.....75

Figure A1.4 A plot showing the atmospheric pressure reading on 30-April-2020 obtained from the Thinnect sensor node located in Rahu, Tallinn.....75

Figure A1.5 A plot showing the relative humidity reading on 30-April-2020 obtained from the Thinnect sensor node located in Rahu, Tallinn.....75
Figure A4.1 Top compartment of the sensor node.....80
Figure A4.2 Complete sensor node.....80
Figure A4.3 Lower compartment of sensor node.....80

List of tables

Table 3.1 Key specifications of the EFR32MG SoC [63].....	29
Table 3.2 Key features of the Thinnect Smart City Gateway [68].....	39
Table A3.1 The sensor node energy consumption and efficiency analysis.....	79

1. INTRODUCTION

Real-time environmental monitoring has been a subject of many research works and city based initiatives. Air pollution for instance, has been a great concern for major cities around the globe. Exposure to air pollution is a public health issue and has been associated with lots of health effects such as cardiovascular and respiratory disease, pregnancy complications, cancer and adverse birth outcomes [1]. This pollution can be made up of Ammonia, Sulfur dioxide, Carbon monoxide, Nitrogen dioxide and fine-particulate matter with diameter less than $2.5\mu\text{m}$ (PM_{2.5}).

According to a study by the World Health Organization (WHO) [2], 92 percent of the world's population is exposed to more than the recommended particle concentrations of ultra-fine particulate matter (PM_{2.5}), which results in 3 million premature deaths yearly. This particle exposure is predominantly high in megacities and can lead to fatal diseases such as stroke, lung cancer and chronic obstructive pulmonary disease [2]. F. Gozzi et al [3] stressed the link between exposure to PM_{2.5} and cardiovascular mortality and morbidity. He indicated that a reduction in particulate matters (PM) levels can help decrease the rate of cardiovascular disease within few years. The health hazard associated with PM exposure is related to the dimension and morpho-chemical features of the airborne particles [4] which depends on the different source or processes emission. Generally, as particles get smaller, they possess the greater chances of reaching the alveolus in the human lungs. Also, particles with high superficial area (irregular particles) can easily absorb cancerogenous and toxic compounds which has adverse effects on human health.

Gas pollutants such as nitrogen dioxide (NO₂) and carbon monoxide (CO) are both respiratory sensitizers [5] and have greater adverse effect on individuals with underlying cardiovascular or respiratory conditions[1]. Exposure to NO₂ is known to affect the proper functioning of the lungs while CO reduces the oxygen carrying capacity of the blood, thus affecting cognitive functions at low concentration and highly toxic at increased concentrations [6].

Another popular environmental condition is the urban-heat-island effect, responsible for megacities being 5-11°C warmer than other surrounding areas. This is often associated with high incidences of heat stroke, dehydration, and cardiovascular and respiratory diseases [7].

It is obvious that this has been a developing problem and the negative impact on our wellbeing is enormous. Although, most developed countries have been achieving significant success in lowering environmental pollution through focused strategies and banning of high polluting industries [8], a considerable percentage of Europeans still live in areas where regulated PM limits are constantly exceeded [9]. A substantial decrease of life expectancy has been observed [10].

Therefore, since the need to have a pollution free environment is inevitable for higher quality of life and human sustainability, it is paramount to raise awareness by constant monitoring of these harmful pollutants and presenting the data in a comprehensive way, in order to assist policymakers and planners in developing and implementing better air quality management plans. This smart city solution should be deployed on a large scale for it to be effective and overcome the limitations of the traditional methods. As such, the proposed system must be simple, cost effective and efficient in terms of both accuracy and power management.

In this thesis, I will improve the functionality of the sensor node developed in the Smart Environment Networking Technologies (SMENETE) project, a cost-effective environmental monitoring system (EMS) suitable for wide area use in a smart city. The sensor node is made up of a compact low-cost system of hardware, firmware and software that has been deployed on a large scale in Tallinn. This system can measure various environmental conditions such as air pollution level (CO, NO₂, NH₃, particulate matters), ambient temperature, pressure and relative humidity. The environmental monitoring system leverages existing Thinnect's proprietary wireless mesh technology to transmit data to the Thinnect cloud solution for data processing, analysis and presentation. This industry initiative based on Tallinn City need was developed in collaboration with researchers in Tallinn University of Technology and Thinnect OU, an IoT Edge of Network Service Provider founded in Tallinn, Estonia.

1.1 Problem statement

The monitoring of environmental pollution using traditional means usually involves having a massive monitoring stations installed. These stations rely on highly accurate and expensive analyzers to measure different environmental gases and other parameters. Although, with this level of accuracy, the installation and maintenance cost is huge as they require frequent calibration, high maintenance

and heavy power requirements. These requirements often limit the possibility of using them on a large micro scale. In recent years, due to the rapid development in the field of micro electronic systems, research institutions and industries are working on developing cutting edge environmental monitoring solutions, with low power requirement (battery powered), low setup cost, maintenance cost and more mobility features [11]. These new stations can be found in different indoor and outdoor environments usually deployed as a wireless sensor network (WSN).

The overall goal of this thesis is to improve the existing sensor node in the SEMENTE project by developing a software driver/firmware that enables the sensor node to acquire data and convert it into quantities that conform with engineering standards. The resulting sensing system from this research work can be used in high density per unit area to provide localized pollution data, as opposed to the existing gigantic pollutant analyzers, which are installed in limited numbers due to the reasons earlier mentioned.

This thesis objectives are:

1. To calibrate the multi-gas sensor used in the sensor nodes of the Environmental monitoring system prototype.
2. To write the driver for the Multi Gas sensor unit in order to acquire data and process it to conform with engineering standards.
3. To analyse the data collected by the existing sensor nodes and validate with the conventional systems.
4. Recommend a power management strategy to improve the energy efficiency of the system.

The city of Tallinn is interested in the results of the project to assist in developing and implementing air quality management plans to maintain concentrations of air pollutants to levels within the limit and target values specified by the EU's air quality directives (2008/50/EC Directive on Ambient Air Quality and Cleaner Air for Europe and 2004/107/EC Directive on heavy metals and polycyclic aromatic hydrocarbons in ambient air [12]).

1.2 Chapters review

This thesis contains 5 chapters. Each chapter is structured as follows.

The first chapter of this thesis covers the introduction, problem statement and thesis objectives. The chapter 2 describes the state of art of air pollution monitoring systems and its building components. It also highlights existing solutions and the need for low-cost solutions. The later part of this chapter talks about the application of wireless sensor networks in environmental monitoring and referenced several research works that employed such architecture.

In chapter 3, the various building blocks of this environmental monitoring system were described in detail. The components of the hardware and software design were analyzed, and specifications given. The sensors implementation and data acquisition processes were also outlined.

Chapter 4 of this thesis covers the detailed description, results and analysis of the work done in this thesis. The calibration process of the multi-gas sensor was discussed in steps while stating the outcome of each step and its significance. The second section gives a general overview of the firmware that was developed to convert the sensor data acquired by the gas sensor to gas concentration in engineering units. This program is written in C-language and is based on the constants and equation derived in the previous section. The following section covers the presentation of the sensor data analysis, observation and validation. The later part of this chapter outlines the current energy conservation of the system and recommends an optimized energy efficiency strategy.

The 5th chapter contains the summary of the activities carried out in the thesis, the result and the conclusion drawn based on the analysis carried out. The later part of this chapter outlines the recommended future work.

This thesis work contains four appendices. Appendix 1 contains additional chart showing the comparison between the sensor data obtained from the Thinnect sensor node located in Rahu and the conventional environmental monitoring station located in Rahu, Tallinn. In appendix 2, the C-program written to convert the sensor data acquired by the MICS-6814 gas sensor to gas concentration in standard engineering unit was given. The last appendix contains the current energy consumption analysis and the expected energy consumption based on the recommended strategy.

2. STATE OF THE ART

2.1 Air pollution monitoring systems

Environmental pollution in cities with pervasive sources of emission has attracted huge global attention owing to the massive impacts on human lives and well-being. Various cities around the world have deployed networks of monitoring stations adopting traditional measurement equipment [13], [14]. These stations boast of measurement capability for a wide variety of pollutants and measurement reliability which aids long-term pollution estimation. The data collected from these monitoring stations can be processed and used to generate a pollution map/model which provides information and prediction of the environmental situation. However, pollution monitoring using these fixed traditional stations has several limitations which includes high installation cost, frequent calibration and high maintenance which inevitably limits their usage on large scale resulting in low spatial resolution of the data, which often leads to inaccurate assessment of the whole area of interest [15]–[17].

Various researchers have also placed environmental sensors in places such as industrial sites and major roads with high traffic to assess the personal exposure to air pollution in these areas [18]–[21]. The measurements obtained from these stations/locations are only able to reflect on the pollution level in their immediate area. In order to estimate the pollutant level at the areas not covered by existing measuring station based on the measured area, a variety of methods have been proposed by researchers e.g spatial averaging, dispersion modeling, nearest neighbor, neural networks, Inverse Distance Weighting (IDW) etc. Most research works estimate pollutant concentrations using a single method [22]–[26], while some studies estimated pollution at different scales by combining several methods [27], [28]. Currently, about 10 conventional monitoring stations have been installed in Tallinn. The environmental pollution data of locations without monitoring stations are obtained by estimations. However, the data from these estimations lack cross-validation and verification.

The advancement in the field of sensing technology, Micro Electro Mechanical Systems (MEMS) and Wireless Sensor Networks (WSN) has led to an increasing use of low-cost portable devices to monitor environmental conditions [29], [30]. This has made it possible for sensors to be deployed in large numbers to address these

prevalent problems of the traditional methods. The existing works can be classified into three categories based on the carriers of the sensor nodes, viz; Static Sensor Network (SSN) the sensor nodes are often mounted on streetlight poles or specially selected locations, Community Sensor Network (CSN) the sensor nodes are usually carried by volunteers or individuals who are interested in environmental monitoring, and Vehicle Sensor Network (VSN) the sensor nodes are carried by vehicles equipped with mobile environmental monitoring stations. These existing works have greatly increased the spatial resolution of the environmental pollution data compared to that of conventional monitoring systems.

These newly developed sensors are usually fabricated using special micro-fabrication techniques and contain MEMS made of microfluidic, nanostructured and optical elements which allows them to be light-weight, compact and inexpensive [31]. These designs are also complemented by sensor circuits that incorporate low-power and energy efficient communication devices. Cutting-edge computing solutions for data handling and a wide range of software solutions for data visualization have made their evolution to be more exciting [31], [32]. There are several categories of low-cost air pollution sensors currently available namely; electrochemical sensors, metal oxide sensors, photo ionization detector, optical particulate counter and optical sensors [33].

2.2 Gas sensors

Gas sensors are used to detect and identify various types of gases. The main parts of sensors are components that respond to changes in chemical or physical properties, and converted to electrical signals by the transducers[31]. These days, there are many different gas detection technologies available, each with certain merits and demerits. Till now, there are five major widely adopted low-cost portable gas sensors, namely: solid state sensors, electrochemical sensors, non-dispersive infrared radiation absorption (NDIR), catalytic sensors and photo-ionization detector (PID) sensors. These sensors are cheap, have fast response time (1/10th seconds or few mins), and light weight (<100g). However, no single type of these sensors can measure all the hazardous gases. Each type has sensitivity to specific kinds of hazardous gases. Although, until now none of the low-cost portable gas sensors have the quality and accuracy of the conventional monitoring apparatus but they offer a decent accuracy and detection range [34]. In addition, these sensors require

calibration (calibration involves exposing the sensor to a specific kind of gas with predefined pollution level, the sensor parameters are adjusted to minimize the difference between the predefined gas concentration and the sensor output) before use and after a given operational period. The need to calibrate and calibration procedures are highlighted in [35].

In this thesis, the goal is to detect hazardous gases CO, NO₂ and NH₃. Merging the characteristics in [34], [36] and the contrasts (as regards detectable gases, cross sensitivity, linearity, power consumption, response time, maintenance and life expectancy), the two best sensors for detecting these types of gases are solid state sensors and electrochemical sensors. The former was selected due to its low cost, low maintenance, portability and high life expectancy.

2.2.1 Solid-state Gas Sensor

The solid-state ambient gas sensors working principle was discovered by scientists while working with semiconductor p-n junctions that are sensitive to environmental gases. A solid-state sensor is made up of one or more metal oxides like aluminum oxide or tin oxide (the metal oxide used depends on the type of gas the sensor is designed to measure), and a heating element. These metal oxides can be made into paste, called bead-type sensor (see Figure 2.1). It can also be deposited on a silica chip which is similar to making semiconductors, called chip type sensor (see Figure 2.2). Exposing these metal oxides to the ambient gases dissociates the gases into charged ions that make the electrons accumulate on the surface of the metal oxides. These accumulated electrons alter the conductivity of the metal oxides. This change in conductivity is used to deduce the concentration of a specific kind of gas. A heating element is introduced to increase the reaction rate which results in a strong electrical signal. This heating element is also used to regulate the temperature because the conductivity change of a particular kind of ambient gas differs with temperature changes. [36]

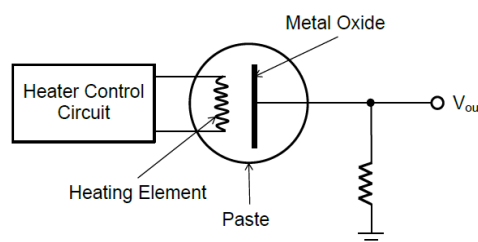


Figure 2.1 A bead-type solid state gas sensor [36].

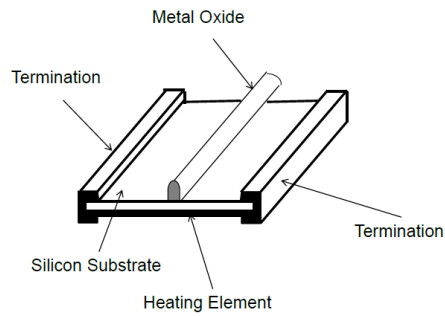


Figure 2.2 A chip-type solid state gas sensor[36].

2.3 Particulate Matter Sensor

Particulate matter (PM) also known as particle pollution is a term used for a mixture of liquid droplets and solid particles in the air. Some of these particles includes visible ones like dust, soot, dirt and invisible ones that can only be detected with electron microscope. PMs are categorized based on size as PM₁₀ (generally 10 micrometers and smaller), PM_{2.5} (with diameters around 2.5 micrometers and smaller) and PM_{1.0}.

Measuring particulate matter (PM) is not a straightforward procedure as there are lots of techniques (used in conventional monitoring systems) available in measuring the mass concentrations of particulate matter. Different measurement methods may give different result, owing to the complex nature of PM [37]. Some conventional monitoring instruments often eliminate the effect of changing humidity and temperature by using a heating element. Conversely, the heating element tends to evaporate the semi-volatile species thereby influencing the measurement results. As a result of this, some instruments make use of a special dryer as opposed to heating element (e.g., the Nafion dryer [38]). The available methods of measuring PM concentration can be classified into two categories. The first one is the direct reading instrument, which provides continuous measurements (with sampling intervals in seconds or minutes) of the PM concentration in ambient air [39]. The other method is the filter-based gravimetric sampler, which works by collecting the PM on top of a filter which requires periodical weighing in the lab. This weighing procedure is a human resource and time-consuming task, which often leads to a huge delay (in days) between data collection and reporting. It is essential to note that these reference methods are not absolute but subject to many artifacts such as temperature and humidity change and semi-volatile compounds. The four common

continuous measurement techniques of PM in ambient air are; Tapered Element Oscillating Micro-Balance (TEOM) Analyzers, β -Attenuation Analyzers, Black Smoke Method and Optical Analyzers [37].

In recent times, there has been a continuous increase in the application of low-cost sensors to PM monitoring [40]–[42]. While they are not as accurate as the professional instruments, their major merits are the low power demand and small dimension. Moreover, this translates to low-cost allowing it to be distributed for large-scale application in handheld devices [43]. When necessary, the low accuracy is enhanced by employing appropriate calibration methods [44]. For example, [45] showed that a dust sensor (Sharp GP2Y1010) can be effectively used for monitoring PM after a thorough calibration. Khadem [46] proposed the use of this same sensor in developing a sensor node to be used in a wireless sensor network (WSN). The data comparison with other professional air quality monitoring systems showed impressive results. Li [47] also developed a low-cost portable indoor air quality monitoring device, the PiMi air box, also based on a cost-effective sensor (the SYhitech DSM501). After calibration, the data provided by the PiMi air box was within the range of the data collected at fixed stations with professional devices owned by government institutions. Hasenfratz [40] showed that, if properly calibrated, the SYhitech DSM501 can satisfactorily measure the concentration of particles $> 2.5\mu\text{m}$ indoor. They also highlighted the necessary hardware required for the real-time availability of data using the wireless technology.

2.4 Wireless sensor network

Due to the fast-technological advancement of wireless technology and embedded electronics, researchers have been showing more interest in Wireless Sensor Networks (WSNs) [48]. A typical WSN is made up of tiny devices known as nodes. These nodes are composed of an embedded CPU with limited processing power and some smart sensors. Using these sensors, the node is able to monitor surrounding environmental variables such as gas concentration, heat, humidity etc. Usually, a WSN node contains computing unit, sensor interfaces, transceiver and power unit. These units carry out the crucial tasks of making the nodes communicate among each other in order to transmit the data polled by their sensors. The necessity of this system leads to the development of the concept of IoT. This concept of IoT makes the immediate access to these environmental data feasible. Such that, the

efficiency and productivity of numerous processes increase dramatically. A typical WSN is made up of 3 major components viz: sensor nodes, gateway and user/backend (observer). Sensor nodes and gateway makes up the sensor field while gateways and observers are connected through a special network usually the internet [39] (see Figure 2.3).

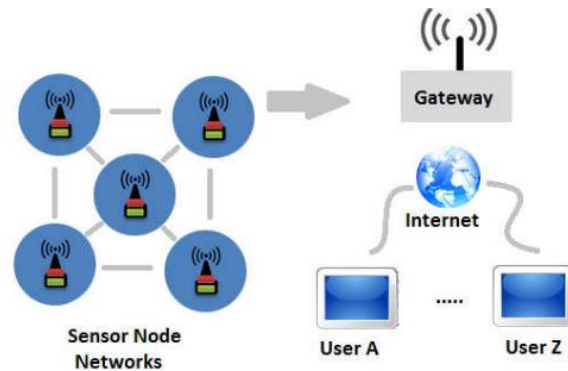


Figure 2.3 Typical architecture of a WSN [39].

A sensor node is a node in a sensor network which has the capability of gathering information from its surrounding environment, processing such information, communicating with other nodes on its network and the data transferred with the support of other nodes via wireless communication channel to the Gateway which routes the data to the cloud, where real-time decision-making takes place.

Each sensor node is constructed uniquely in accordance with its environment. For example a sensor installed in a marine environment [49], [50] will have their enclosure designed to withstand the effects of salinity, moisture and should be water proof. The tougher the environment's effect on sensors, the more robust the mechanical and electronic designing. While the risk of environmental interference is high in urban areas, the suburban and rural environments cause less distortion to wireless communication [51]. The high congestion and noise pollution associated with the increasing population in the urban areas is the major cause of interference. Technological improvements which aim at minimizing cost, low energy consumption and easy deployment are actively being researched. The use of WSN in urban environment has gained so much acceptance leading to its use in numerous unconventional applications. WSNs are being deployed for intelligent monitoring of water level, humidity, temperature strength of mega structures, pressure, vehicular activities on the road, criminal surveillance on streets, remote monitoring of patient's health status and a wide variety of other applications [52], [53]. WSNs have also been deployed for Hazardous gas monitoring in sewers, sewage flood

monitoring, as a disaster relief strategy [54], [55].

Lots of research works have been done to measure air quality using wireless sensor networks and IoT [11], [56]. These works involve measuring different types of air pollutants using either stationary or mobile sensors. For instance, the University of Patras carried out a power consumption evaluation of the Wasp mote platform in [57]. This platform was implemented using the Libelium Wasp mote Plug & Sense! model known as Smart Environment PRO [58]. The paper identified critical processes and implementing of a system for measuring power consumption in WSN. In another research project, the University of Armed Forces developed a wireless system for measuring air quality [59]. The study delivered a hardware, software and firmware solutions for air quality measurement. This was achieved using an Arduino platform consisting of sensor nodes which were connected to internet via a network gateway. The system measured carbon dioxide (CO₂) and carbon Monoxide (CO) in the city of Quito, Ecuador.

In [60] a peer-to-peer based WSN was deployed to monitor air pollution in east London where air quality has worsened for some time. MoDisNet is a WSN that consists of static and mobile sensor nodes deployed based on the Enhanced Science (e-Science) grid infrastructure. The sensor nodes are built on the GUSTO technology which makes use of ultraviolet radiation to determine the contents of pollutant gases like NO_x, CO₂, O₃, Benzene and SO₂ etc. Distributed clustering was implemented to guarantee optimal network performance as data mining is carried out so that the gathered information can be analyzed. Jung [61] have deployed a geo-sensor network which monitors air pollution in order to take pollution mitigation steps. The project involved installation of 24 sensors for monitoring dust, wind speed and direction, humidity, CO₂, ultraviolet radiation, altitude and other parameters. 10 routers were deployed to route information to the control server. This server is responsible for context aware analysis and presents the pollution statistics via graphical user interface which has the capability of alerting the user of near future air pollution hazards. For example, fire and smoke warning or possibility of a dust storm in a location. The pollution prevention procedure is to warn the building manager of a potential air pollution and close the windows by enabling the window actuators.

In [62], using WaspNet architecture, an ubiquitous sensor network was implemented to monitor air pollution in Cape Town, South Africa. The innovative features of WaspNet are effective data dissemination, readiness for deployment

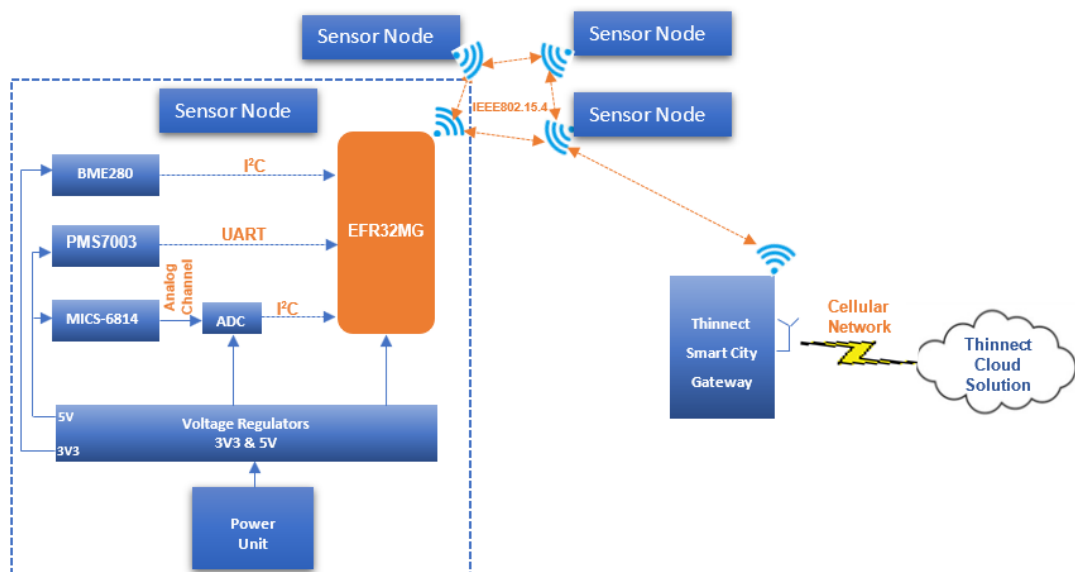
over a long distance and security. The sensor node was called Waspote, monitored pressure, temperature, humidity, methane, CO₂, ammonia and additional 8 gases. The data collected was delivered to the users through Google Maps. Information propagation was accomplished by using ZigBee and GSM technologies.

In this thesis, the sensor nodes developed leverage on the existing Thinnect wireless mesh network. This mesh network uses Thinnect's proprietary communication protocol running on 802.15.4 physical layer which had been deployed in Estonia for various smart city applications. This approach coupled with the implementation of low power sensor nodes will ensure that the initial and maintenance cost of this environmental monitoring system is highly effective and economical.

3. METHODOLOGY AND DEVICE DEVELOPMENT

3.1 General overview of the environmental monitoring system

In this project, a system level approach was used. The system is custom solution previously developed within the scope of the SMENETE project. It was implemented by integrating individual hardware components on a custom PCB. The system consists of a sensor node which is made up of three ambient sensors, a 32-bit Microcontroller (MCU), and a power management unit. The PMS7003 sensor measures the level of the fine particulate matter (PM1.0, PM2.5 and PM10) in the air. The relative humidity, pressure and temperature data are captured by the BME280 sensor. The last sensor is the MICS-6814 multi gas sensor which measures the pollution level of our gases of interest namely; Carbon monoxide (CO) and Nitrogen dioxide (NO2). These sensors were hooked up to the powerful low energy Silabs Mighty Gecko 32-bit system on chip (EFR32MG12). The EFR32MG12 has an integrated radio transceiver which enables sensor nodes to form a multi-hop mesh network via Thinnect’s proprietary communication protocol running on 802.15.4 physical layer and connects to the Thinnect Smart City Gateway. This gateway achieves external communication via GSM communication and transmits the data to Thinnect cloud platform for further data processing and analysis. This chapter illustrates the hardware and software architectures, how these components were integrated together and configured to create the system used in data capturing, processing and transmission. The architecture of the system is illustrated in the block diagram in Figure 3.1 below.



27
Figure 3.1 The architecture of the Environmental Monitoring System

3.2 Hardware Architecture

The hardware infrastructure of this system can be broken down into five parts which are explained below.

3.2.1 Silabs Mighty Gecko 32-bit SoC

The EFR32MG is an energy-friendly system on chip (SoC) that combines a 32-bit MCU based on an ARM Cortex-M4 processor with a highly integrated radio transceiver. This MCU is well suited for battery-operated application and systems requiring high performance and low energy consumption. The EFR32MG SoC has a wide range of functionality down to their sleep modes with current consumption at sub-microamp level which makes it highly energy efficient. With Low Energy Sensor Interface (LESENSE), the EFR32MG can duty-cycle resistive, capacitive and inductive sensor while autonomously operating in Deep sleep mode. The EFR32MG also boasts of a feature known as Peripheral Reflex System (PRS). This feature provides a communication channel that allows different peripherals to have a direct connection between each other and enable them to communicate without CPU intervention and wake up. These characteristics coupled with other energy efficiency capabilities while delivering incredible performance, makes the EFR32MG very useful in applications like this that require high performance with strict energy budget.

[63]

The EFR32MG SOC at low level can be broken down into 8 categories namely; the core and memory, energy management, timers and triggers, clock management, serial interfaces, analog interfaces, I/O ports, and security modules. The EFR32MG system architecture is shown below in Figure 3.2.

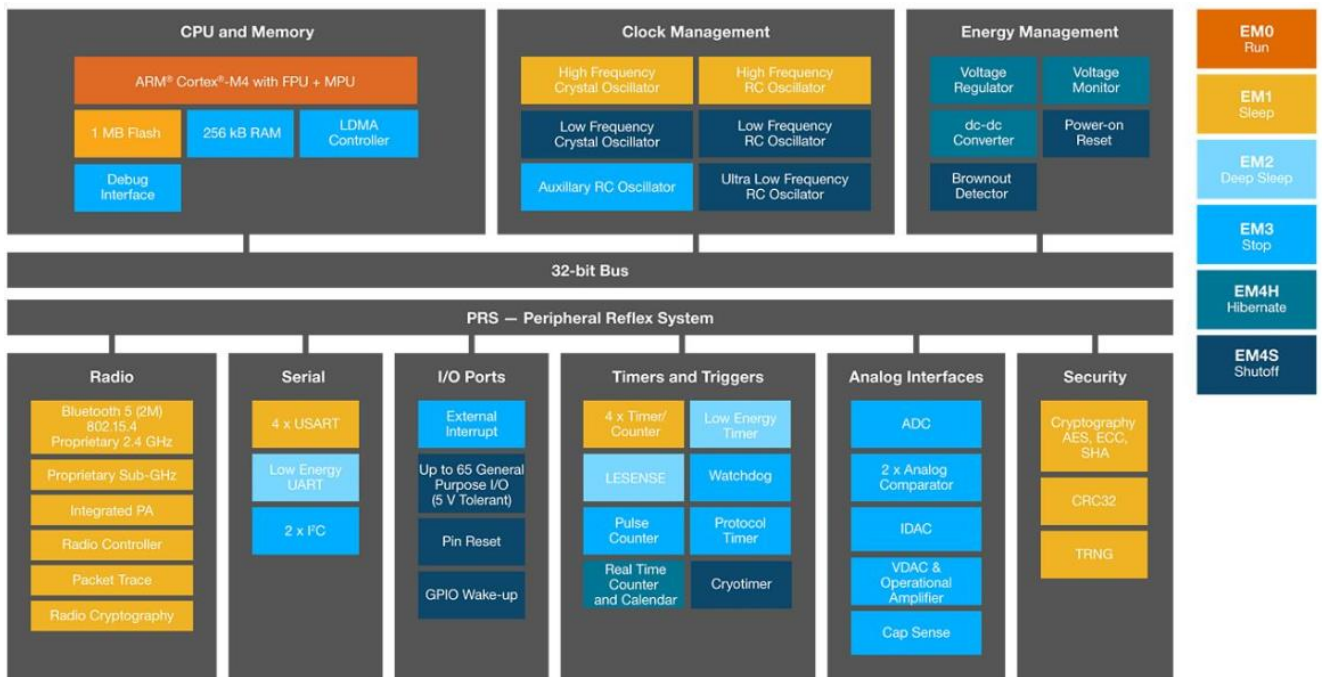


Figure 3.2 The architecture of the EFR32MG SoC [63]

To allow the EFR32MG operate and take advantage of the ultralow power architecture, it can operate with a main input clock rate of 4 MHz -40 MHz and integrates a low and ultralow frequency clocks. In addition to clock rate and CPU flexibility, the MCU offers 1024kB flash program memory, 256kB RAM data memory and other needs such as RTOS implementation. This SoC also features a highly configurable radio transceiver with an antenna interface that supports a wide range of wireless protocol such as Zigbee, Bluetooth Low Energy (BLE) and Thread. This integrated radio transceiver was used to establish a wireless communication with the Thinnect Smart City Gateway via the IEEE802.15.4 physical layer [63]. Key specifications of this chip can be found in Table 3.1 below.

Table 3.1 Key specifications of the EFR32MG SoC [63]

MCU Core	ARM Cortex-M4
Core Frequency (MHz)	40
Flash (kB)	1024
RAM (kB)	256
Receive Sensitivity	-102.7 (250 kbps O-QPSK DSSS)
Max Output Power	19
GPIO	31
Temperature (Min) – (Max) (°C)	-40 to 85
Package Type	QFN48

Zigbee Capable	Yes
Thread Capable	Yes
Bluetooth Low Energy Capable	Yes
2.4 GHz Capable	Yes

3.2.2 PMS7003 Particle Concentration Sensor

PMS7003 is a real-time optical particle counter (OPC). It is a digital and universal particulate matter sensor which can be used to estimate the number of suspended particles in the air and transmit over a digital interface. This sensor can be integrated into various instruments used in environmental improvement to provide correct concentration data in real time. The data from the PMS7003 particle sensor is transmitted in real-time to the EFR32MG MCU over the universal asynchronous receiver and transceiver (UART) interface.[64]

PMS7003 Particle Concentration Sensor Working Principle:

The PMS7003 is a particle sensor based on optical sensing technology. This type of sensor usually makes use of the laser scattering principle. This sensor produce scattering by making use of laser to radiate suspending particles in the air, these particles cause scattering (or absorption) of the incoming light at a certain degree and changes with time. This is detected by a photodiode and converted into real-time particle count and mass concentration value by the integrated microprocessor based on Mie theory [64].

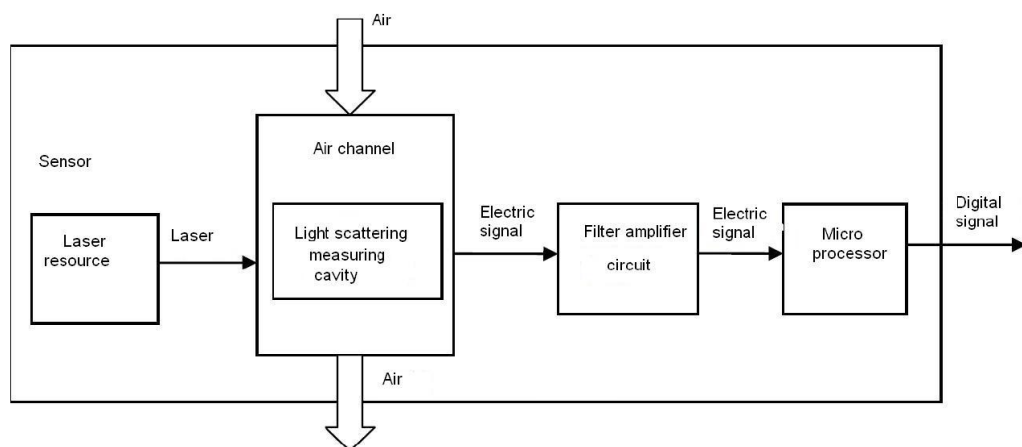


Figure 3.3 Functional block diagram of the PMS7003 particle sensor [64].

PMS7003 Particle Concentration Sensor Operation:

The PMS7003 particle sensor comes with an integrated circuit. The internal circuitry is shown in Figure 3.1 above. The sensor output (Particle size) is transmitted over a serial interface (UART). To integrate the sensor on our custom PCB, the manufacturer’s datasheet was consulted, and the typical circuit recommended is as shown in Figure 3.4 [64] while our final PCB implementation circuit is as shown in Figure 3.5 [65] below.

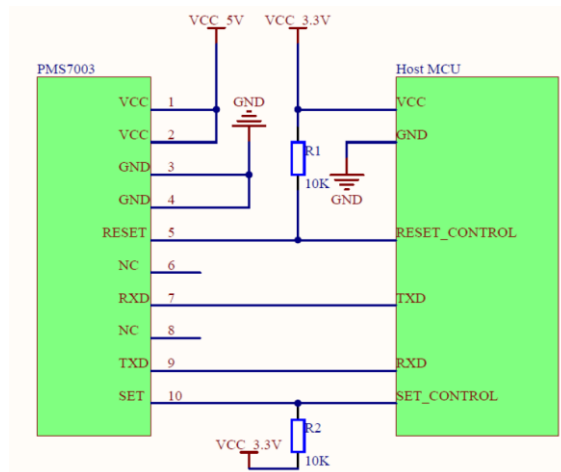


Figure 3.4 The schematic diagram of PMS7003 particle sensor [64].

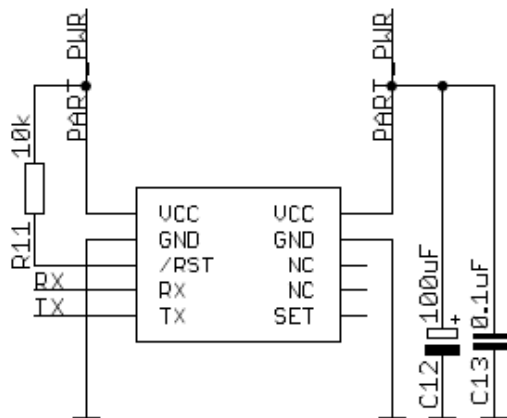


Figure 3.5 The implementation architecture of the particle sensor on PCB [65].

The PMS7003 sensor circuit is powered by a 5V power supply because the internal fan operates at this voltage level. The high level of the serial data pin is 3.3V, as such no level conversion is required because the MCU operates at this voltage level. The serial data pins transmit (TX) and receive (RX) were connected to the MCU for data exchange. The Reset pin (RST) is in use, so pull up is required according to the manufacturer. C12 and C13 acts as a buffer for sensor supply circuit.

The output of the sensor transmitted over the serial interface is the quality and number of each particles with different size per volume. The unit volume of particle number is 0.1L while that of mass concentration is $\mu\text{g}/\text{m}^3$. The output works in two modes namely; passive and active. The default mode of the sensor after power up is the active mode. In this mode, the sensor sends serial data automatically to the host MCU. This mode is divided into two sub modes namely: stable and fast mode. The sensor runs in the stable mode at an interval of 2.3s if the particle concentration change is small. However, if the concentration change is much, the sensor automatically runs at fast mode with an interval of 200-800ms. In summary, a higher concentration leads to a shorter interval.

3.2.3 MICS-6814 Multi gas sensor

The MICS-6814 is a compact semiconductor metal oxide (SMO) sensor with three independent sensing elements in a single package. SMO gas sensors are one of the most researched group of gas sensors due to their size dependent properties. Most SMOs have a size in the range of 1nm-100nm. The principle behind this gas sensor is that when the detecting layer (made of metal oxide) is exposed to the target gases, it alters the resistivity of the layer. This way, the gas sensor act as a variable resistor whose value depends on the concentration of the target gas exposed to. The resistance increases for oxidizing gases such as Nitrogen dioxide (NO_2) or Ozone (O_3) while it reduces for reducing gases such as carbon monoxide or Volatile organic compounds (VOCs). In simple terms, the reducing gases eliminate some of the insulative oxygen species on the detecting layer causing the total resistance to go down while the oxidizing gases add more insulative oxygen thereby increasing the resistance.

The above reactions above occur at increased temperatures and thus, the detecting layer needs to be properly heated with the MICS-6184 integrated heater. One of the main advantages of this sensor over other ones in the market is that the heating power required to run the sensor is far less (about 40mW). It should be noted that

the rate of change of the sensor resistance with respect to the gas concentration doesn't not have a linear relationship. As such, it was required to establish a polynomial equation that shows this relationship which was subsequently integrated into a firmware.

MICS-6814 Multi gas sensor operation

The MICS-6814 is sold as a bare sensor. As such it was required to first to connect to a PCB and the circuit integrated according to the manufacturer's datasheet. A 5 volt power supply is needed but the heater circuit needs a series resistor to prevent the sensor from overheating. The measuring circuit also requires a series resistor to facilitate the measurement and limit the voltage across the detecting layer. The manufacturer's recommended supply circuit is shown in Figure 3.6 [66] while our sensor implementation circuit on PCB is as shown below in Figure 3.7 [65].

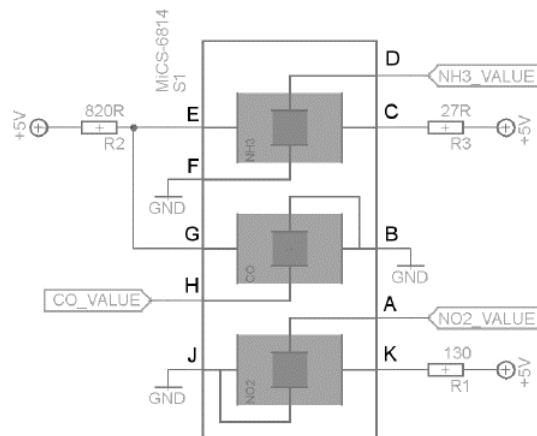


Figure 3.6 The MICS-6814 multi gas sensor power supply circuit recommended by the manufacturer [66]

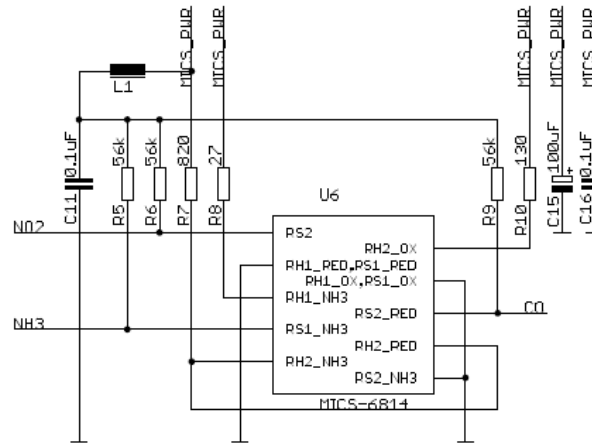


Figure 3.7 The implementation of the The MICS-6814 multi gas sensor power supply on PCB [65]

As shown in Figure 3.7 above, the measurement of the sensor resistance R_s for each channel labelled (NH3, NO2 and CO) was achieved by connecting a 56k Ω resistor in series with the sensor. Based on the principle explained earlier, the sensor resistance changes based on the concentration of gas it is exposed to. A change in sensor resistance directly leads to change in the voltage drop across it. This voltage across the sensor can now be used to determine the actual resistance of the sensor and it's measured by a 10bit Analog-to-Digital converter (ADC) and connected to the MCU over Integrated to Integrated circuit (I2C) interface. I2C is a serial communication protocol used between integrated circuits such as a MCU and set of relatively slower peripherals. I2C is a 2-wire serial bus developed by Philips, widely used for interconnection of single chip MCU, memory chips, ADC and variety of other peripheral devices in short distance intra-board communication. This protocol supports multi master and multi slave configuration. Each slave device is identified by the means of 7-bit or 10-bit address through which the master communicates with it. The 2-wires are the Serial clock line (SCL) for clock synchronization and the Serial data line (SDA) for data transfer. Both signal lines are pulled up to the supply voltage by default and are in open drain mode.

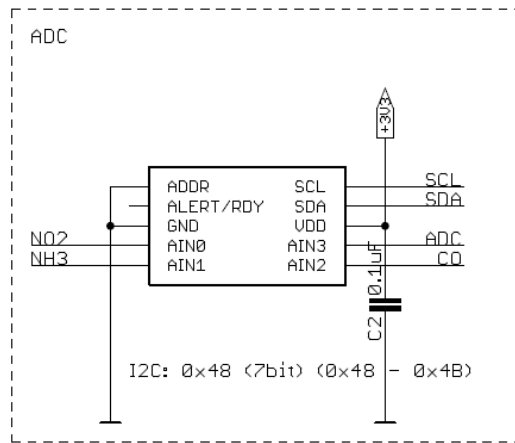


Figure 3.8 The schematic showing how the ADC chip was interfaced with the MICS-6814 multi-gas sensor [65].

When the MICS-6814 is powered up, it needs sometime to setup its chemical equilibrium. This is needed because of the chemical compounds being absorbed and desorbed on the detecting layer after which the resistance stabilizes. The higher the temperature the faster the rate of stabilization. As such, the sensor is initially pre-heated at higher voltage to achieve stability before the voltage is subsequently reduced. Generally, a better precision is achieved with a longer warm up [66].

MICS-6814 Multi Gas Sensor Calibration

The MICS-6814 can measure multiple gases namely Carbon monoxide (CO), Nitrogen dioxide (NO₂) and Ammonia (NH₃). This is possible because it has three fully independent sensing layer integrated in one package. Therefore, there's a need to calibrate each of these layers on the individual target gas. Each sensing layer has different resistance in air and this resistance changes with respect to the concentrations of the target gas. As such, to convert this resistance readings to concentration, it was necessary to derive a calibration relationship (curve) for each target gas. This required measuring the resistance in air at several gas concentrations over the chosen range [66]. The graphical relationship between the sensing resistance and concentration of gas in parts per million (PPM) is according to the manufacturer is given in Figure 3.9 and 3.10 [66]. The calibrating procedures can be found in [66] and results are described in chapter 4.

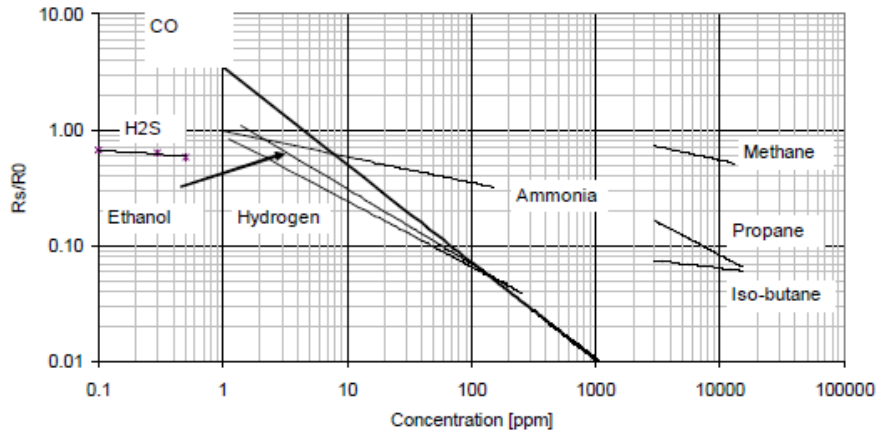


Figure 3.9 The relationship between the concentration of gas in PPM and the ratio of current sensor resistance (R_s) to base sensing resistance in synthetic air (R_0) for reduction sensor (CO_2 , NH_3) [66].

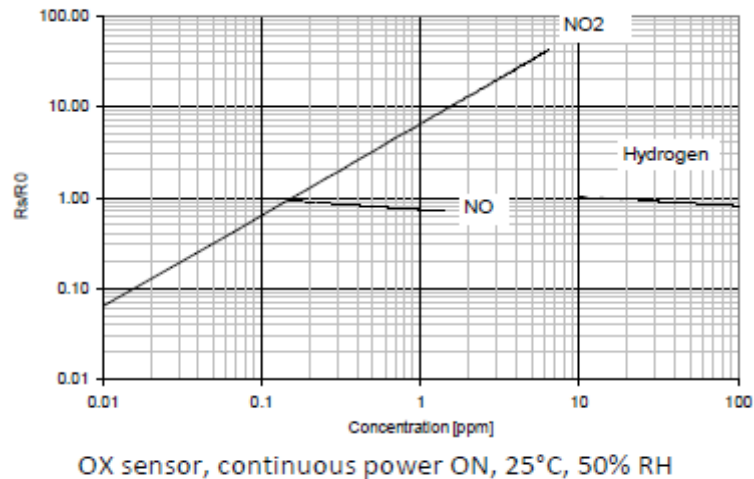


Figure 3.10 The relationship between the concentration of gas in PPM and the ratio of current sensor resistance (R_s) to base sensing resistance in synthetic air (R_0) for oxidation sensor (NO_2) [66].

3.2.4 BME280 Digital Humidity, Pressure and Temperature sensor

The Bosch BME280 sensor is an environmental sensor that can measure humidity, pressure and temperature. This sensor was designed for mobile applications, wearables and other applications where size and power consumption are key requirements. This sensor is a perfect choice for this project due to its ability to achieve high performance, high linearity and accuracy even at low current consumption and total cost of ownership. The BME280 provides digital output over both Serial Peripheral Interface (SPI) and I²C interface. The latter was considered in

this project due to its ease of integration with our existing communication interface. The sensor can be supplied with 1.71V to 3.6V for the sensor supply V_{DD} and 1.2V – 3.6V for the interface supply V_{DDIO} . It can be operated in three power modes namely; sleep, normal and forced mode. The sensor consumes as low as 0.1 μ A while in sleep mode. The BME280 has various power optimization possibilities which can be tailored to the user needs [67]. One of such is the ability of the user to select data rate (based on application) to further optimize current consumption. Figure 3.11 [67] below shows the simplified block diagram of the Bosch BME280.

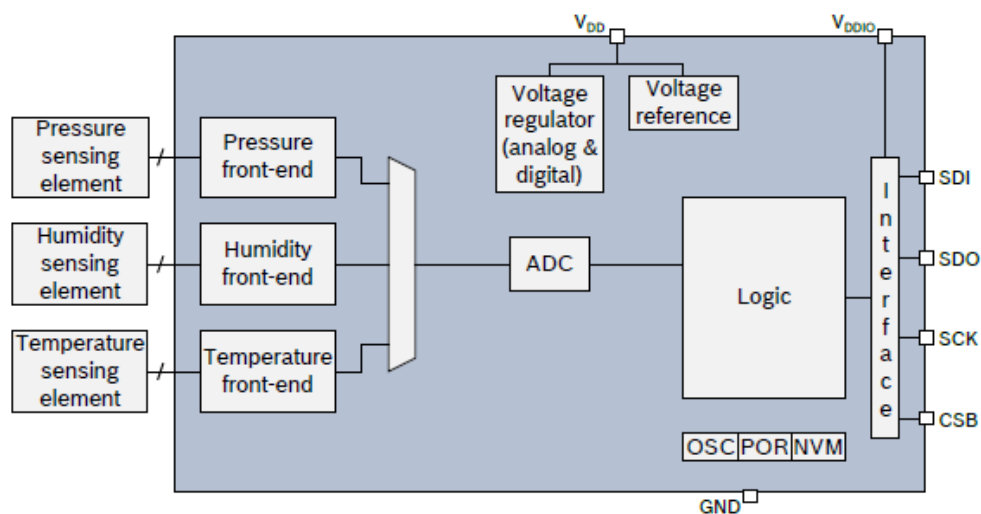


Figure 3.11 The block diagram of the BME280 humidity, pressure and temperature sensor [67]

The BME280 has two different power supply pins V_{DD} and V_{DDIO} . The V_{DD} is the main power supply that powers the internal digital and analog functional blocks while the V_{DDIO} is used to supply the digital interface. As shown in Figure 3.12 below, the V_{DD} and V_{DDIO} pins were connected to a 3.3V supply. The digital interface pins SDI, SDO, SCK and CSB are used for data communication. These data pins can be used as a slave for either SPI or I²C data communication.

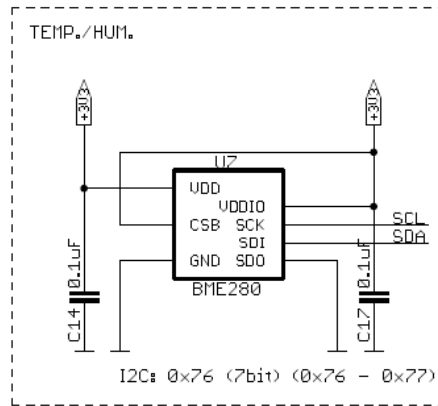


Figure 3.12 The schematic showing how the BME280 humidity, pressure and temperature sensor was integrated on the PCB [65].

In this project, the I²C communication mode of the BME280 sensor was used. To achieve this, the CSB (chip select) pin was pulled up by connecting to V_{DDIO}. The serial clock (SCK) and serial data input (SDI) pins were connected to the SCL and SDA pins of our MCU respectively for data exchange. The SDO is grounded which corresponds to an I2C slave's address of 0x76 as per manufacturer's recommendation. C14 and C17 act as a buffer for sensor supply circuit.

3.2.5 Thinnect Smart City Gateway (TSCG)

The Thinnect smart city gateway is a proprietary gateway by Thinnect OU. It establishes internet connectivity for Thinnect wireless Smart City controllers and sensor mesh network to transmit operating rules to the network, receive sensor data and status information from the network. The sensor node developed in this research work communicates with the TSCG via IEEE802.15.4 standard based radio communication protocol operating at 2.4GHz with a standard data rate of 250kbps. The gateway is installed within the coverage of the sensor node to ensure reliable communication with the nodes. TSCG establishes external communication via GSM communication, as such, the desired local service provider with coverage in the deployed area was installed [68]. The gateway is smart; it has the capability to buffer data and instructions to and from the backend. It ensures the instructions from backend to nodes are executed by continuously retrying until successful. It also buffers data received from nodes and ensures transmission to the backend. TSCG features are highlighted in Table 3.2 [68] below.

Table 3.2 Key features of the Thinnect Smart City Gateway [68].

Electrical characteristics	
Operating voltage	100 - 275 V, 50 - 60 Hz
Power consumption of the control unit (max)	2,4 W
Protection Class	Class II
Mechanical characteristics	
Dimensions	201x89x51 mm
Operating conditions	
Operating temperature	-40°C to +60°C
IP protection rating	67
Communication interfaces	
For Thinnect mesh network	IEEE802.15.4 standard based radio, operating at 2.4 GHz, 16 channels, 250kbps standard data rate.
Network security	160 bit ECC and AES-128
GSM data communication standard	3G (UMTS/HSPA)
SIM card type	microSIM
Wired connectivity (optional)	Ethernet

3.2 Software Design

3.2.1 General overview of software architecture

This phase provides the description of tools and procedures that forms the software architecture of this system. Figure 3.13 below shows the system software architecture.

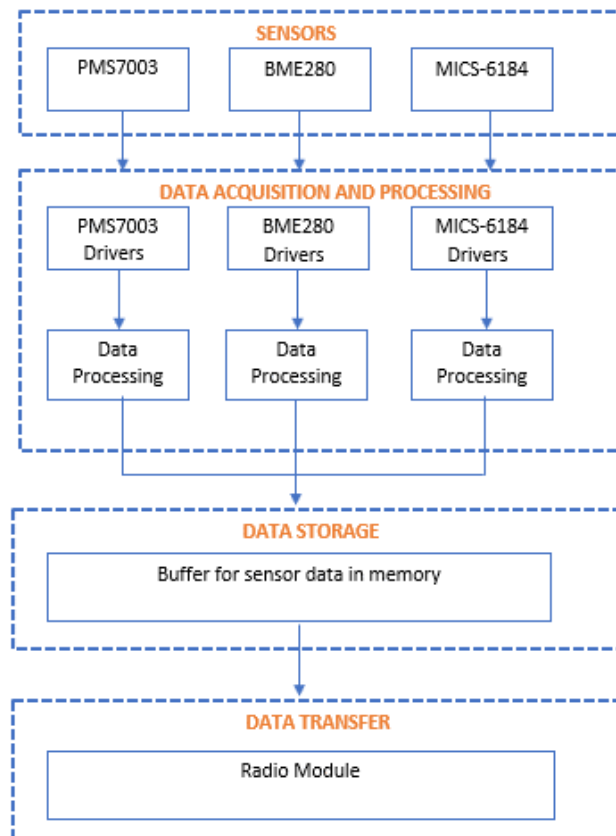


Figure 3.13 The software architecture of the environmental monitoring system

All environmental monitoring sensors used in this application work as input devices, and they are connected to the EFR32MG MCU via different digital data communication protocols such as I2C, UART. The MCU retrieves the data from the connected sensors, processes and then proceeds to transmit it via its integrated radio module to the nearest available node in the mesh network. This data hops in the network until it gets to the node closest to the Thinnect Smart City gateway which subsequently forwards the received data to the Thinnect's cloud platform for further data processing and analysis.

3.2.2 Data acquisition from sensors and transmission

Reading data from the sensors and processing

The EFR32MG MCU runs a Realtime operating system and Thinnect's networking stack application. It is programmed using an integrated development environment (IDE) based on Eclipse known as Simplicity studio. It is Silicon Lab's flagship development environment for IoT system design based on their 8-bit and 32-bit MCUs, sensors and Wireless SoC. The IDE provides an integrated set of tools that allow developers to access and configure various peripherals registers of the MCU using an application programming interface (API).

The PMS7003 particle sensor transmits the particle sizes through its UART interface. The MCU interfaces with this sensor via the Universal Synchronous Asynchronous Receiver/Transmitter (USART) interface. A USART interface is a serial I/O interface which allows for full duplex synchronous or asynchronous communication. The synchronous mode requires a separate line to transmit the clock signal with the data while the asynchronous mode doesn't require a separate clock signal. In a UART (asynchronous) communication, it is required that both the transmitter (in this case, PMS7003) and receiver (MCU) are to agree on the baud rate, word length and stop bit to exchange a UART frame. According to the PMS7003 datasheet, its default baud rate is 9600bps, word length of 8-bits and a stop bit of 1. To allow the MCU read data from the PMS7003 particle sensor, the MCU USART interface was configured by using the USART API provided by IDE to set the mode of operation (as asynchronous), the word length and stop bit in the USART control register and program the baud rate in the UART baud rate register as recommended in the sensor data sheet.

As described in the hardware architecture, the MICS-6814 gas sensor is an integrated sensor that consists of three fully independent sensors in one package. The sensor detecting layers experience a change in resistance based on their level of exposure to the target gas. The output of the sensor has three channels (as shown in Figure 3.6) which corresponds to each detecting layer. Each channel is connected in series with a 56k resistor to a 5V supply. The voltage across each sensor is passed into different channels of the 10-bit ADC whose digitized output is interfaced with the MCU over I2C. This ADC is an I2C slave with an address of 0x48. To retrieve data from this I2C slave, the IDE offers series of APIs to carry out such operation by passing the slave I2C address, data register and the size of data to read.

As earlier stated, the digitized data read from the 10-bit ADC connected to the MICS-6814 sensor corresponds to voltage level across the sensor in digital form. This digitized data is converted to resistance by a function written in the MCU that applies the formula in Equation 3.1 above. By following the procedures in highlighted in Chapter 4, a base resistance (R_o) was determined for each gas ($CO = 88.66k\Omega$, $NO_2 = 6.2k\Omega$, and $NH_3=69.9k\Omega$). This base resistance R_o is the resistance of the sensor when exposed to an ideal environment during calibration, and it's fixed until the sensor is recalibrated. The ratio of the sensor resistance in current environment (R_s) to this established base resistance (R_o) is the variable ($x = R_s/R_o$) needed determine the current concentration of the target gas in PPM. Having established these relationships in Section 4.1 as equations 4.4, 4.5 and 4.6 for CO, NO₂ and NH₃ respectively, a function was created to implement these equations and return the level concentration of each gas (in PPM) for the current sensing environment. See Appendix 2 for code implementation.

Reading from the BME280 Digital Humidity, Pressure and Temperature Sensor was also done over the I2C protocol. The output of this sensor is the relative humidity, pressure and temperature (in %RH, Pa and °C respectively) of the current sensing environment. This I2C slave has an address of 0x76. To retrieve data from this sensor, the IDE provides series of APIs to carry out such operation by passing the slave I2C address, data register and the size of data to read.

Transmitting data to the Thinnect smart city gateway and to Thinnect cloud solution

The sensor nodes form a multi hop mesh network using the Thinnect proprietary communication protocol running on 802.15.4 physical layer. Each sensor node transmits its data (and data received from other nodes) to the closest node in the mesh network. The node closest to the Thinnect smart city gateway routes received packets to it. The connection between the gateway and the cloud platform is established using Thinnect proprietary stack of network applications leveraging on open source protocols such as RESTful API, RabbitMQ etc. Thinnect cloud solution is a proprietary cloud solution developed by Thinnect OU. Each node can be configured from the cloud platform. Configuration such as specifying how frequent node should sample and transmit data and many other functionalities can be activated from the backend.

4. RESULTS

This chapter describes the procedures taken in calibrating the multi-gas sensor, the calibration coefficients derived, analysis of the captured data (before and after sensor calibration), comparison of results with the one from existing stations and the power efficiency recommendation.

The first section of this chapter describes the steps taken in calibrating the multi-gas sensor and the outcome of the calibration. The calibration process was used to derive calibration constants and equations. These relationships form the basis for the firmware that was written in the subsequent section. The third section outlines the data analysis and comparison of the existing sensor node data with conventional systems. Lastly, a recommendation was given on how to further optimize the energy efficiency of the system.

4.1 Calibrating the MICS-6814 Multi Gas Sensor

The MICS-6814 multi gas sensor can measure three gases namely; Carbon monoxide (CO), Nitrogen dioxide (NO₂) and Ammonia (NH₃). Each gas is detected by a different sensing layer. As such, each layer was calibrated individually. The calibration procedure can be found in the sensor datasheet [66].

Firstly, it was required to establish the relationship between the 10-Bit ADC digital output values and the sensor sensing resistance. This relationship was subsequently used to derive the base sensing resistance (R_o). R_o is the resistance of the sensor when exposed to clean air under controlled ambient conditions. This controlled ambient conditions requires exposing the sensor to synthetic air at $23 \pm 5^\circ\text{C}$ and $50 \pm 10\%$ RH for Reduction sensor (CO and NH₃), and synthetic air at $23 \pm 5^\circ\text{C}$ and $<5\%$ RH for Oxidation sensor (NO₂) [66].

The calibration procedure was concluded by deriving three equations which show the relationship between the sensing resistance ratio (R_s/R_o) and the actual gas concentration in PPM. The concentration of each target gas in parts per million (PPM) has a relationship (although not linear) with the ratio of the sensor resistance in current environment (R_s) to sensing resistance in synthetic air (R_o) as sketched on the graphs in Figure 3.9 and 3.10. R_s being the sensor resistance in the current

environment while R_o is the sensor resistance derived when it was exposed to clean air.

4.1.1 Deriving the relationship between ADC digital output value and sensor resistance

In order to determine the R_o , it was first required to establish the relationship between the ADC digital output value and the resistance of the sensor (which corresponds to the current level of concentration of exposed gas). This relationship is dependent on the voltage divider ratio. The manufacturer stated the sensor resistance range in the datasheet as 100-1500k Ω for the CO sensor, 0.8-20k Ω for the NO₂ and 10-1500k Ω for the NH₃ sensor [66].

The ADC digital output corresponds to the voltage across the sensor. Since we have a fixed resistance of 56k Ω in the measuring circuit (Figure 4.1), we can therefore determine the sensor resistance by applying the voltage divider rule. An equation was derived to calculate the sensing resistance in real time, based on the values received from the ADC digital output. The derivation of this equation is as shown below, and it was subsequently implemented in the C-program written in Appendix 2.

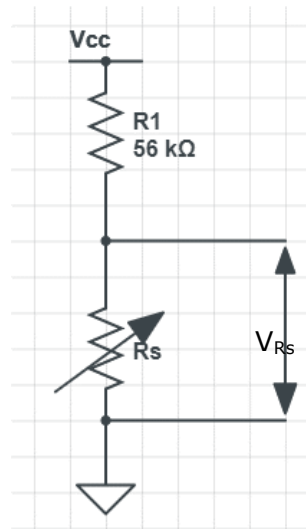


Figure 4.1 The circuit diagram for determining the sensing resistance of MICS-6814 multi gas sensor.

Considering the circuit connection for determining the resistance of the multi-gas sensor shown in Figure 4.1 above, the relationship between the voltage across

sensor (V_{RS}) (which is connected to the ADC channel input) and sensor resistance (R_s) can be derived using the voltage divider rule as:

$$V_{RS} = V_{CC} * \frac{R_s}{R_s + 56k} \quad 4.1$$

By making R_s subject and rearranging equation 3.1, we get:

$$R_s = \frac{56k * V_{RS}}{V_{CC} - V_{RS}} \quad 4.2$$

The voltage (V_{RS}) is the voltage across the sensor and it is the analog signal connected to the input channel of the ADC. The ADC converts it to a digital form and outputs via its output channel. The applied voltage (V_{CC}) is the maximum input of the ADC.

Equation 4.2 can be rewritten as:

$$R_s = \frac{56k * ADC_{CurrentReading}}{ADC_{MaxReading} - ADC_{CurrentReading}} \quad 4.3$$

Where;

- R_s is the sensor resistance based on the target gas concentration.
- 56k is the value of the resistor connected in series with each sensor channel.
- $ADC_{CurrentReading}$ is the ADC digital output which corresponds to the present voltage across the sensor (V_{RS}) in digital form.
- $ADC_{MaxReading}$ corresponds to the maximum digital output of the ADC, in this case our ADC is 10-bit. Therefore, the maximum ADC level is 2^{10} which equals 1023.

4.1.2 Deriving the base sensing resistance in air (R_o)

Having established the above relationship in Equation 4.3, the sensor was exposed to synthetic air and the ADC value measured were 627 for CO, 102 for NO₂ and 568 for NH₃. The base sensing resistance (R_o) was subsequently calculated for each of these gases as shown below;

From Equation 4.3 above;

$$R = \frac{56k * ADC_{CurrentReading}}{ADC_{MaxReading} - ADC_{CurrentReading}}$$

Therefore, to establish Ro for CO, convert ADC value of 627 to resistance by applying Equation 4.3;

$$R = \frac{56k * 627}{1023 - 627}$$

$$R = 88.66k\Omega$$

Applying the above approach to other target gases, the base resistance (Ro) for CO, NO2 and NH3 sensors were found to be 88.66k Ω , 6.2k Ω , and 69.9k Ω respectively.

4.1.3 Deriving the relationship between sensor resistance ratio (Rs/Ro) and the gas concentration in PPM

This task was carried out to determine the relationship between sensor resistance and the concentration of each gas (in PPM). According to the sensor datasheet, the relationship can be determined using a graph (Figure 3.9 and 3.10) above. This graph shows how the ratio of two resistances (Rs/Ro) translates to the concentration in PPM of the target gas. This can either be done manually on the graphs or by establishing a mathematical relationship. To automate this process, a mathematical formula to determine this relationship was derived which was subsequently implemented in the software code in appendix 2 for gas calculation in real time.

In order to derive the relationship, several data points were manually taken for each line in the graph (see Figure 3.9 and 3.10) that corresponds to our target gas (CO, NO2, NH3). These carefully selected points from the graphs were put into three different two-column spreadsheets. The two columns represent the resistance ratio and corresponding PPM value for each target gas. Subsequently, a graph was plotted for each gas. The X-axis represents sensor resistance ratio representing the X-axis while Y-axis is the corresponding PPM) and a trend line generated (Figure 4.2, 4.3 and 4.4). The trend line equation shows the mathematical relationship between sensor resistance ratio (Rs/Ro) and the gas concentration in PPM.

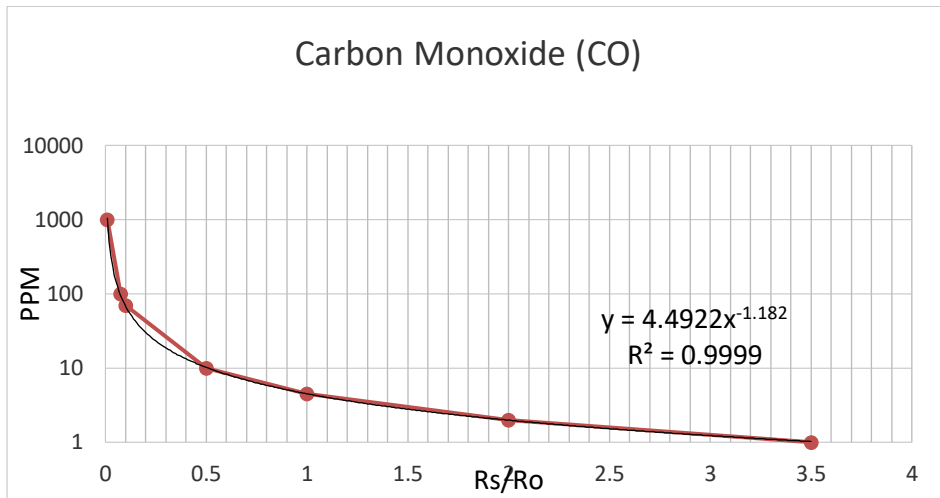


Figure 4.2 A plot showing the relationship between PPM and sensor resistance ratio (Rs/Ro) for CO

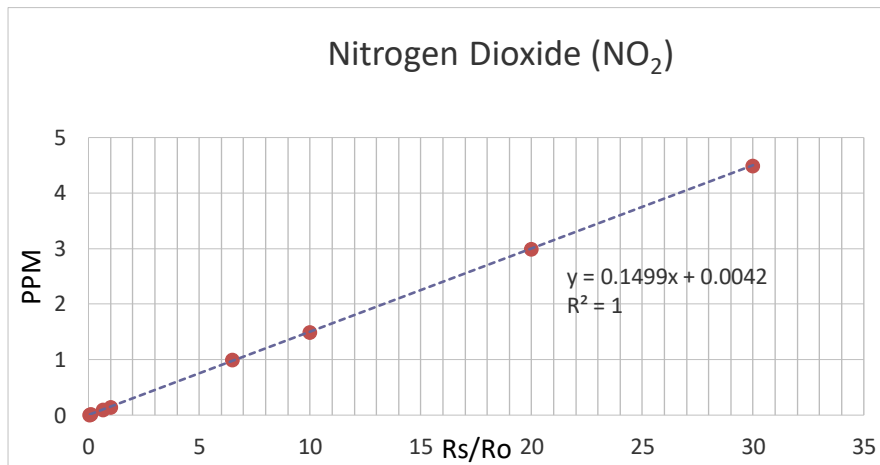


Figure 4.3 A plot showing the relationship between PPM and sensor resistance ratio (Rs/Ro) for NO₂

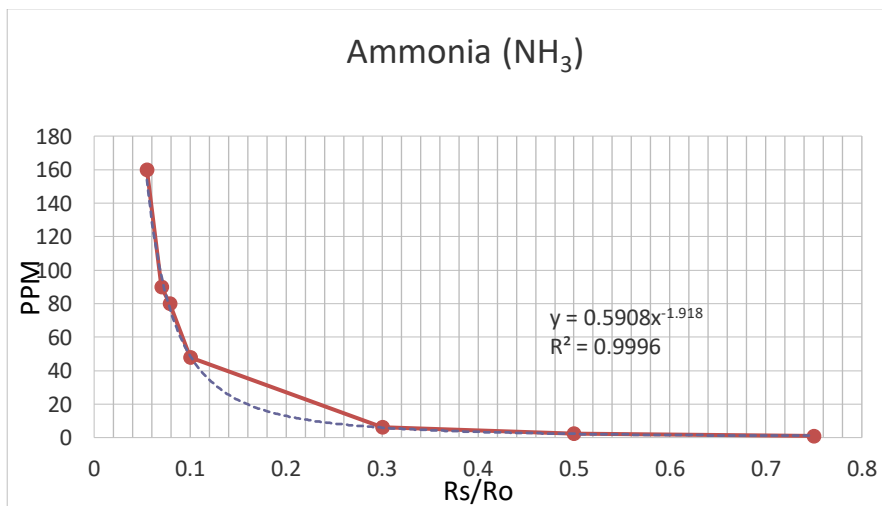


Figure 4.4 A plot showing the relationship between PPM and sensor resistance ratio (Rs/Ro) for NH₃

From the above Figure 4.2, 4.3 and 4.4, the relationship between the sensor resistance ratio (R_s/R_o) and the concentration of each target gas in PPM was derived by displaying the trendline equation of each figure in excel. The relationship are as follows:

$$\text{Carbon Monoxide (CO in PPM)} = y = 4.4922x^{-1.182} \quad 4.4$$

$$\text{Nitrogen Dioxide (NO}_2 \text{ in PPM)} = y = 0.1499x + 0.0042 \quad 4.5$$

$$\text{Ammonia (NH}_3 \text{ in PPM)} = y = 0.5908x^{-1.918} \quad 4.6$$

Where;

- y is the concentration of the gas in PPM and
- x is the sensor resistance ratio R_s/R_o .

The above equations were implemented in the software developed in Appendix 2 to calculate the real-time gas concentration level based on the sensor resistance.

In summary, this section shows the multi gas sensor calibration and procedure. The relationship between the ADC values and the current sensing resistance (R_s) was first derived in Equation 4.3. Subsequently, the base sensing resistance (R_o) was also determined as $88.66\text{k}\Omega$, $6.2\text{k}\Omega$, and $69.9\text{k}\Omega$ for the CO, NO₂ and NH₃ sensors respectively. The calibration procedure was concluded by establishing the relationship between the sensing resistance ratio (R_s/R_o) and the actual gas concentration in PPM. Each gas has a unique relationship, as such, three different polynomial equations were derived and stated in Equations 4.4, 4.5, and 4.6. The code implementation is given in Appendix 2.

As a further step in calibration, the system will be deployed next to one of the existing conventional stations in the city of Tallinn. The initial result will be checked and some compensation in the system software will be implemented, if required.

4.2 Firmware development for the Multi Gas Sensor

Having derived the calibration constants and equations in the previous section, a C-program was written to implement the solution. This solution includes, getting the current sensor resistance in air and converting it to standard engineering units in real-time.

The development environment was setup in the Eclipse Integrated Development Environment (IDE). A header file was created to store the functions declaration and constants used in the main program. The main program consists of two functions.

The first function named `getSensorRs()` is responsible for calculating the current sensor resistance. This function takes a character as an argument. This argument corresponds to the name of the sensor whose current resistance should be returned. Depending on the desired sensor, a switch statement is evaluated. This switch statement calls the function responsible for getting the current ADC value. The returned ADC value is converted to resistance in the latter part of the function by applying the Equation 4.3 derived in sub-section 4.1.1 above. The `getSensorRs()` function returns the calculated resistance as the current sensor resistance.

A second function `calGas()` converts the current sensor resistance to gas concentration level in PPM. This function takes the gas name as an argument. Depending on the gas specified, the function first calculates the resistance ratio (R_s/R_o). This is achieved by dividing the current sensor resistance (the returned value of `getSensorRs()`) by the already established sensor base resistance (R_o) (see sub-section 4.1.2). The result of this operation is the resistance ratio and it is stored in a variable (`ratio_gasName`). Subsequently, a switch statement is evaluated based on the desired gas name. The switch statement calculates the gas concentration level by applying the either of Equations 4.4, 4.5 and 4.6. The `calGas()` function returns the calculated gas concentration in PPM.

As described above, the complete code can be found in the Appendix 2 for further reference.

4.3 Analysis of Data collected by sensor nodes and validation

4.3.1 Overview of system implementation

The actual system prototype is as shown in Figure 4.5 below (More pictures of the sensor node can be found in Appendix 3). The system has 2 compartments. The lower compartment houses a PCB that has all the sensors integrated on it. The upper compartment contains the battery and a PCB that has the EFR32MG12 chip and power controllers integrated on it. The two sections are interconnected together via eight wires carrying two different digital signals (I2C and UART) and power. The enclosure is strong enough to withstand harsh weather conditions as it is expected to be deployed outdoor for a long period of time. These sensor nodes are mounted street lighting poles and distributed across several locations in Tallinn.



Figure 4.5 Environmental monitoring system prototype.

The data for two Thinnect sensor nodes stationed at two different locations in Tallinn (Liivalaia and Rahu) are presented in this thesis. Our target environmental parameters include particulate matters (PM10, PM2.5, and PM1), ambient temperature, relative humidity, atmospheric pressure, carbon monoxide (CO) and nitrogen dioxide (NO2). These locations were chosen because they have existing

conventional environmental monitoring stations installed within their proximity and the data are publicly available. Data were obtained from these conventional stations to validate the ones obtained from our sensor nodes' cloud platform. The results for Liivalaia station are presented below for each of the parameters measured while that of Rahu can be found in the Appendix 1.

4.3.2 Data analysis and validation of Thinnect's sensor node around Liivalaia station

A sensor node was deployed within the proximity of an environmental monitoring station in Liivalaia, situated close to Hotel Olympia bus stop in Tallinn. The data collected were extracted and results presented below.

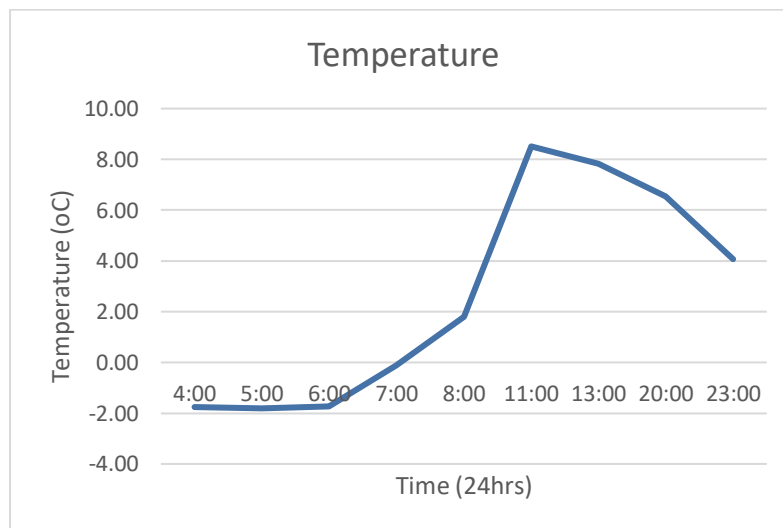


Figure 4.6 A plot showing the temperature reading on 30-April-2020 obtained from the Thinnect sensor node located in Liivalaia, Tallinn.

The temperature chart in Figure 4.6 above is a plot of the data obtained from the Thinnect's sensor node. It corresponds to the hourly average temperature in the Liivalaia region between 4:00 and 23:00 on 30th April 2020. According to the chart, temperature was at its lowest (-1.81°C) around 5am and peaked (8.51 °C) for the day at 11am. Unfortunately, the conventional station within this location does not capture the ambient temperature, atmospheric pressure and relative humidity readings. In order to validate the results, I compared it with the data obtained from

a public weather information source [69] for the same period. The data from this public weather source shows that the lowest temperature for 30th April 2020 in Tallinn was -3°C while 7°C was the highest temperature. This shows the Thinnect sensor node reading has percentage error of about 21%.

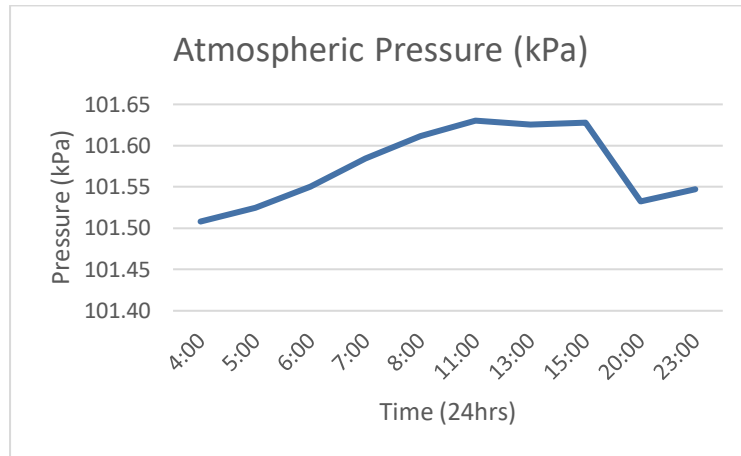


Figure 4.7 A plot showing the atmospheric pressure reading on 30-April-2020 obtained from the Thinnect sensor node located in Liivalaia, Tallinn

Figure 4.7 above, shows the atmospheric pressure reading, as expected, there was not much changes in pressure. Peak atmospheric pressure of 101.68kPa was recorded between 11:00 and 15:00 while it was lowest in early and late hours of the day. A comparison with the public data at [69] shows that the highest atmospheric pressure of 101.5kPa was recorded between 12:00 to 18:00 while the lowest of 101.3kPa was between 00:00 to 18:00. That is a percentage error of less than 0.2%

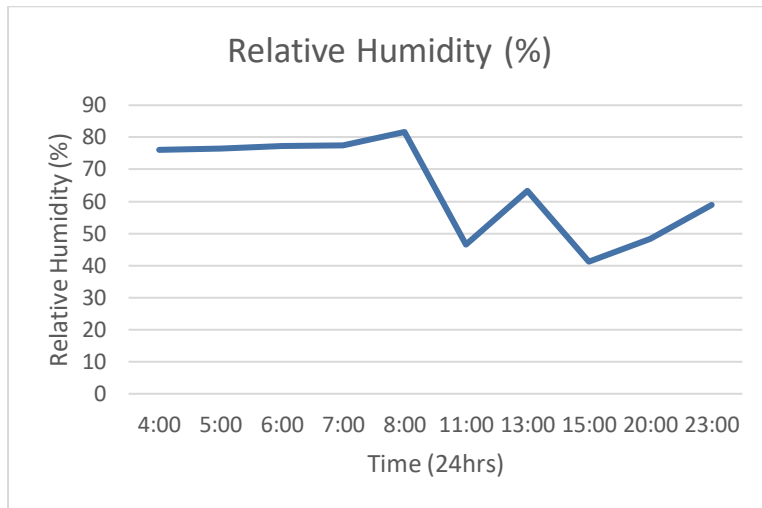


Figure 4.8 A plot showing the relative humidity reading on 30-April-2020 obtained from the Thinnect sensor node located in Liivalaia, Tallinn

The relative humidity chart in Figure 4.8 above shows relative humidity obtained from the Thinnect’s sensor node to have attained approximately 81% at 8:00 while it was lowest at 15:00. Comparing this with the public data archive at [69] for the same period, relative humidity peaked at 95% between 0:00 to 6:00 while it was lowest between 12:00 to 18:00 at 50%. This corresponds to a percentage error of about 15%.

The results above show that the BM280 Temperature, Humidity and Pressure sensor has a percentage error of 21% and 15% in the measurements of temperature and relative humidity respectively. This error can be attributed to the difference in measurement location. The data used for validation is an average of these conditions for the whole of Tallinn and not for the exact location which the sensor node was deployed. Therefore, the variation was anticipated and acceptable for this study.

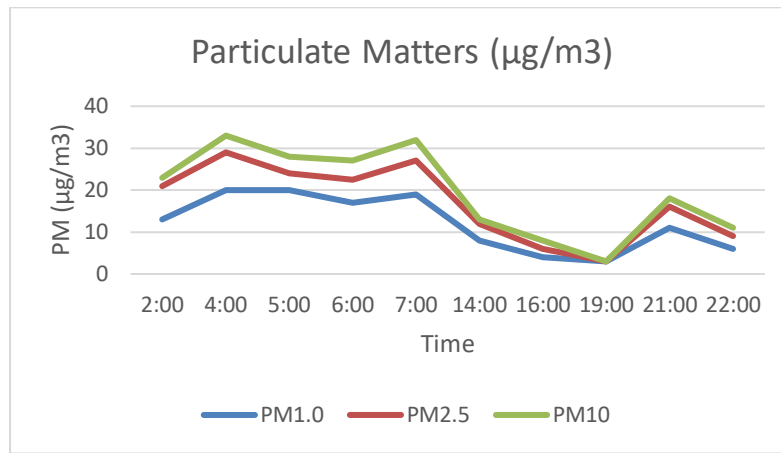


Figure 4.9 A plot showing the Particulate Matters reading on 30-April-2020 obtained from the Thinnect sensor node located in Liivalaia, Tallinn chart for 30-April-2020.

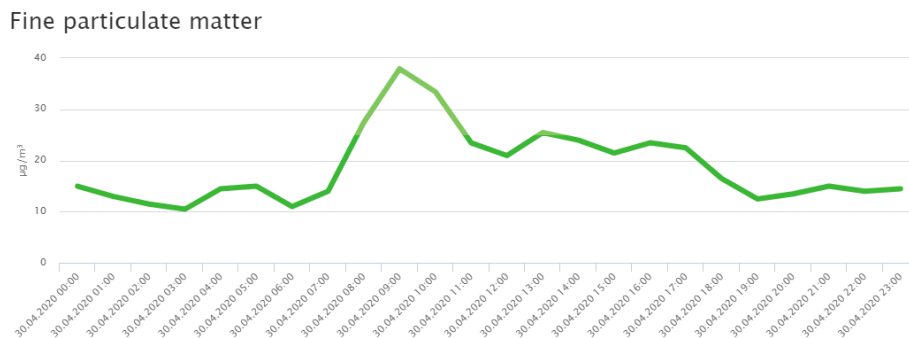


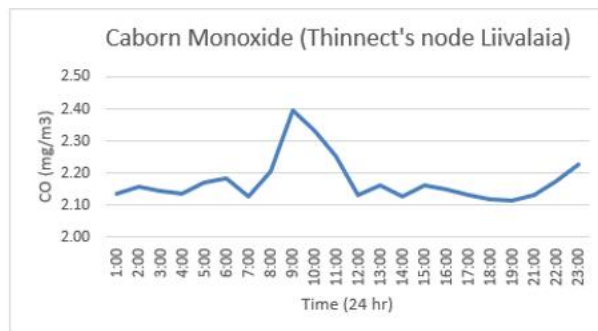
Figure 4.10 A plot showing fine Particulate Matter (PM10) chart for 30-April-2020 from the conventional environmental monitoring station located in Liivalaia, Tallinn [70].

Figure 4.9 above represents a plot of particulate matter of sizes 1, 2.5 and 10 micrometers obtained from the Thinnect’s sensor node. Fine particulate matter (PM10) peaked at $32\mu\text{g}/\text{m}^3$ and ultrafine particulate matter (PM2.5) at $29\mu\text{g}/\text{m}^3$. The Tallinn Environmental Monitoring station at Liivalaia only has record for PM10 which is shown in Figure 4.10 [70]. This data from this station shows that PM10 peaked at $37.9\mu\text{g}/\text{m}^3$ on the same day under consideration.

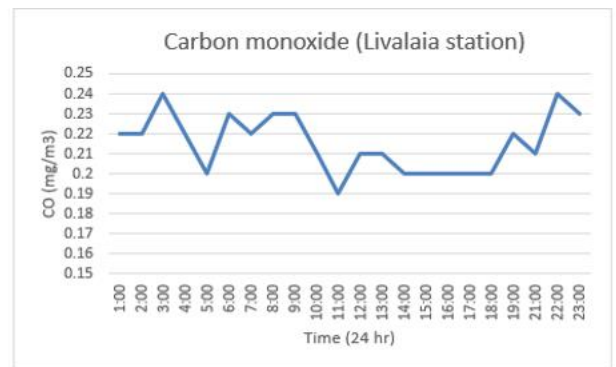
In summary, the PMS7003 particulate matter sensor performed fairly well but it occasionally gave some questionable data. For example, there were few sudden spikes recorded in the particulate matter readings and became low the next few minutes. Just as every system requires continuous improvement, this is one key areas of this system that needs to be further investigated.

Analysis of the MICS-6814 multi gas sensor data obtained from the Thinnect Node at Liivalaia (applying calibration coefficient) Vs data from the conventional station at Liivalaia.

In this sub-item, the calibration coefficient obtained in Sub-section 4.1.2 was applied to the raw ADC data obtained from the MICS-6814 multi gas sensor in the Thinnect node at Liivalaia. This was done in order to convert the already captured data to their respective gas concentration units. The resulting gas concentration were compared to the ones obtained from the conventional station at Liivalaia. To carry out further validation, an independent standalone multi gas sensor node was introduced. This standalone sensor node is made up Seedstudio grove multichannel gas sensor and Arduino microcontroller unit. Details of my findings are presented below.



A plot showing the Carbon Monoxide reading on 30-April-2020 obtained from the Thinnect sensor node located in Liivalaia, Tallinn.



A plot showing the Carbon Monoxide reading on 30-April-2020 obtained from the conventional environmental monitoring station located in Liivalaia, Tallinn.

Figure 4.11 Two plots showing carbon monoxide level on 30-April-2020 obtained from the Thinnect sensor node versus the conventional air monitoring station located in Liivalaia, Tallinn.

Figure 4.11 shows two separate plots. The first one represents the carbon monoxide level recorded on 30 April 2020 by the Thinnect sensor node located at the Liivalaia station while the right plot represents the data recorded by the conventional station at Liivalaia for the same period. A comparison of these two plots shows that the data recorded by the Thinnect node doesn't correlate with that of the Liivalaia station. However, looking at the trend, both figures have some correlation. For example, both stations recorded uptrends in the CO level at 2:00-3:00, 5:00-6:00, 7:00-8:00, 21:00-22:00 while recording downtrends at 3:00-4:00, 6:00-7:00, 9:00-11:00, 13:00-14:00. The difference in the values could be as a result the chosen calibration coefficient, distance of Thinnect node from the conventional station or difference in mounting elevations. While experimenting with the Thinnect

node's multi-gas sensor calibration constant, I realized that choosing a $R_o=12.5k\Omega$ instead of $88.9k\Omega$ reduced the percentage error in readings to about 12%. See Figure 4.12 below for the result of the experimental calibration constant.

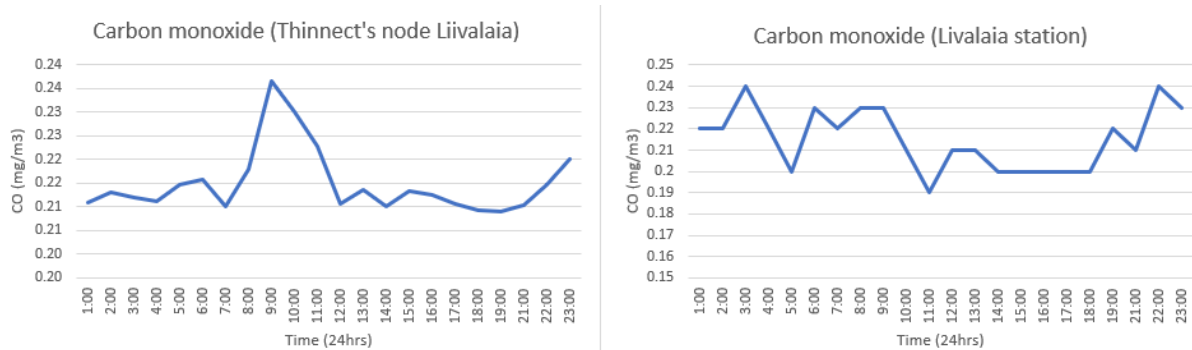
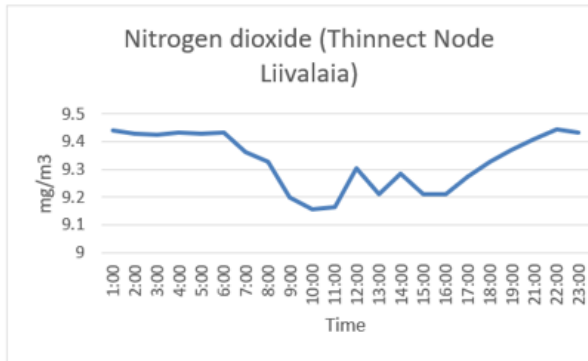
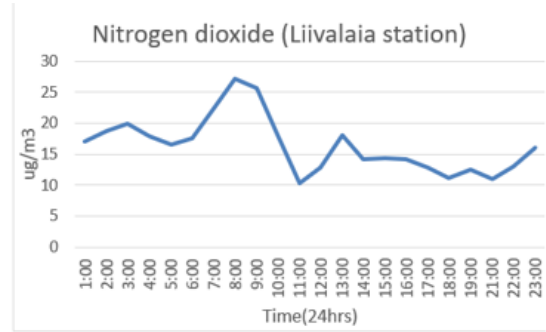


Figure 4.12 A side-by-side comparison of charts showing carbon monoxide level on 30-April-2020 obtained from the Thinnect sensor node (using the experimental calibration constant, $R_o=12.5k\Omega$) versus the conventional air monitoring station (right chart) located in Liivalaia, Tallinn.

This new calibration constant was also applied to the data obtained from Thinnect node located in Rahu and a similar reduction in the percentage error was observed. What I deduced from this is that, getting the right calibrating constant may be dependent on the environment in which sensor is calibrated and deployed. That is, sensor should be calibrated in an environment similar to where it will be eventually installed.



A plot showing the Nitrogen dioxide reading on 30-April-2020 obtained from the Thinnect sensor node located in Liivalaia, Tallinn.



A plot showing the Nitrogen dioxide reading on 30-April-2020 obtained from the conventional environmental monitoring station located in Liivalaia, Tallinn.

Figure 4.13 A side-by-side comparison of charts showing nitrogen dioxide level on 30-April-2020 obtained from the Thinnect sensor node (left chart) versus the conventional air monitoring station (right chart) located in Liivalaia. Tallinn.

In the Figure 4.13 above, the left plot represents the plot for the carbon monoxide level recorded by the Thinnect node on 30 April 2020 while the second plot represents the data recorded by the conventional station at Liivalaia for the same period. The first observation from this figure is that the two readings are expressed in different units. NO₂ is typically measured in $\mu\text{g}/\text{m}^3$. The plot for the conventional station is expressed in $\mu\text{g}/\text{m}^3$ while that of the Thinnect node is presented in mg/m^3 . The reason for this is because, converting the data point from the Thinnect node from mg/m^3 to $\mu\text{g}/\text{m}^3$ will result in a multiple of 1000 (e.g $9.3\text{mg}/\text{m}^3 = 9300\mu\text{g}/\text{m}^3$). This implies the difference between the data obtained from the Thinnect sensor node and the conventional station at Liivalaia is in thousands. This clearly shows something is wrong somewhere. Experimenting with the Thinnect node multi-gas sensor calibration constant did not help to bring down this value.

To further investigate why these values are that high, I configured a standalone multi gas sensor node. This standalone sensor node was made up of a Grove multichannel gas sensor manufactured by Seeedstudio and an Arduino microcontroller. The Grove multichannel gas sensor has the capability to measure multiple gases including carbon monoxide and nitrogen. This sensor was calibrated from Seeedstudio's factory. The new standalone sensor node was deployed for data capturing on 6th May 2020. A plot of the data captured is presented below.

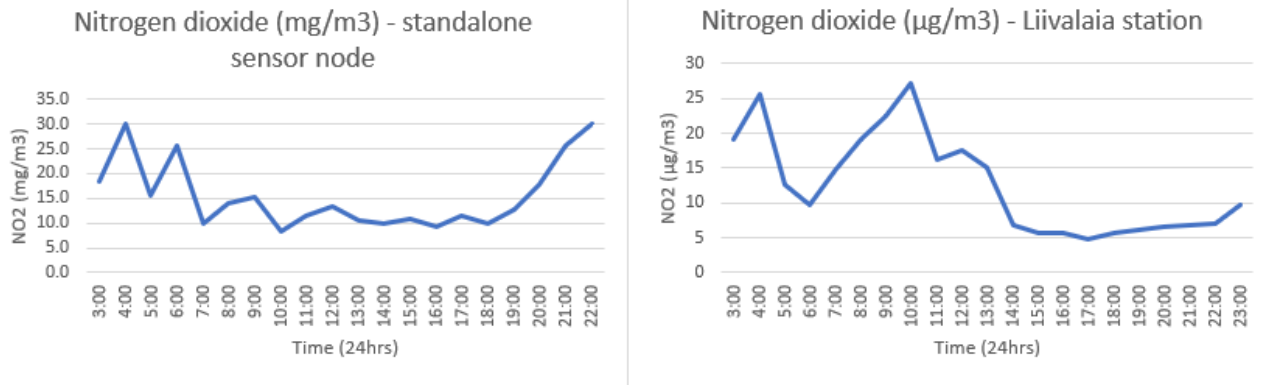


Figure 4.14 Side by side comparison of the nitrogen dioxide level on 06-May-2020 obtained from the standalone sensor node (mg/m³) versus the conventional NO₂ air monitoring station (µg/m³) located in Liivalaia, Tallinn.

In the Figure 4.14 above, the left plot represents the plot for the carbon monoxide level recorded by the new standalone node on 06-May-2020 while the second plot on the right represents the data recorded by the conventional station at Liivalaia for the same period. The data obtained from the standalone sensor node is in (mg/m³) while the conventional station is in (µg/m³). Converting one of the datapoints from the standalone sensor node for mg/m³ to µg/m³, e.g 30mg/m³ = 30000 µg/m³. This result further raises a question on the accuracy of the units in which the conventional station at Liivalaia expresses nitrogen dioxide. Could it be that the scale of the conventional station at Liivalaia is just showing µg/m³ whereas the actual data is in mg/m³? Or the multi-gas sensors used (on both Thinnect node and the standalone sensor node) are not capable of measuring nitrogen dioxide concentration?

After carefully analyzing the data from the different two different Thinnect sensor nodes used in data capturing, I can reach a conclusion that by compensating for the error in the readings of the MICS-6814 multi-gas sensor, it can reliably measure the carbon monoxide level at less than 15% percentage error. This compensation includes reducing the calibration constants used in the data conversion as shown in Figure 4.12 above. Other factor that could be compensated for is the effect of ambient conditions such as temperature, relative humidity and pressure.

These factors are important because the multi-gas sensor uses a change in its resistance to calculate the apparent gas concentration level. Due to this, changes in the ambient temperature will likely cause an apparent change in the resistance of the sensor, thereby influencing sensor response and measured gas concentration significantly. Humidity and pressure will also affect resistance, but the impact of these conditions is likely to be smaller compared to those caused by temperature changes. These effects can be compensated for in the software of the system.

Furthermore, the capability of the multi-gas sensor in measuring nitrogen dioxide

level is questionable. Further investigation needs to be carried out to ascertain why the difference between the two portable sensor nodes (Thinnect and the standalone node) and the conventional environmental monitoring station is in the range of thousands.

4.4 Energy efficiency recommendation

One of the biggest challenges of Wireless sensor/IoT nodes is the issue of energy efficiency. Choosing a low power Microcontroller (MCU) and sensors is the first step towards having a power efficient sensor node. This was already considered in the choice of MCU and sensors used in this environmental monitoring system. For example, the EFR32MG12 SoC is an ultra-low power system-on-chip while the sensors are energy efficient. Furthermore, the system currently switches voltage level from 3.3V to 5V only when required and usually operates in low-power mode.

Nevertheless, there's always room for improvement. Energy efficiency is a function of both power consumption and time. The choice of hardware greatly influences the power demand of a system. The choice of hardware has already been implemented for this system under consideration. As such, the only variable we can optimize is the total on-time of this system. (e.g how long should we keep the system on, over a 24-hours period). Such decision often depends on the use case of a system. Currently, the sensors are constantly turned on and data acquisition and transmission take place every two mins. This frequent transmission of data is not required for this kind of application because the difference in the data acquired within this short interval is insignificant. As such, sensor data should be polled less frequently. A recommend data acquisition and transmission interval will be once every hour. This will allow the node to remain in a sleep or idle state until data capturing is required. An exception to this hourly sampling of data is the multi-gas sensor. The manufacturer recommends that the sensor is preheated for about 20-30 minutes before it is sampled. As highlighted in Chapter 3, preheating plays a huge role in sensor data precision and accuracy. Due to this, it is recommended that the multi-gas sensor wakes up 30 minutes earlier than the other sensors. The chart in Figure 4.15 below shows that implementing this energy strategy will improve energy efficiency of the system by about 75% daily. The basis of this estimation can be found in Appendix 3.

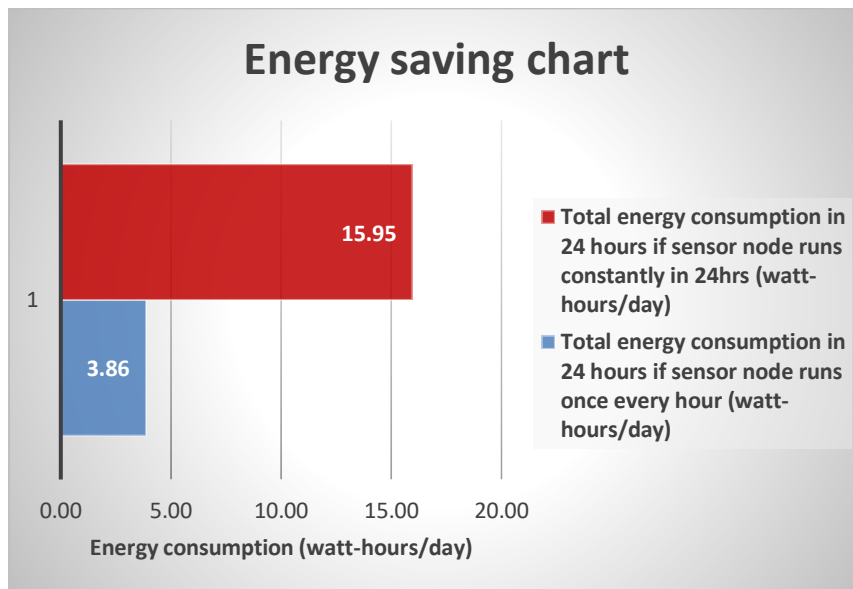
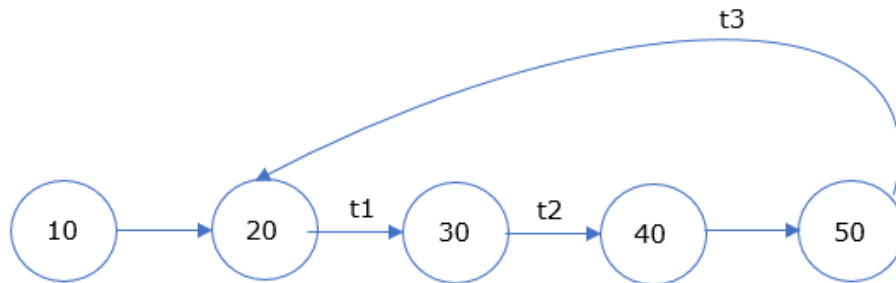


Figure 4.15 A chart showing the current total energy consumption of the Thinnect sensor node watt-hours/day (red) versus the estimated total energy consumption in watt-hours/day (blue) if this recommendation is implemented.

The Figure 4.15 above shows a chart comparing the current total energy consumption of the Thinnect sensor node in watt-hours per day against the estimated energy consumption in watt-hours per day if the above recommendation is implemented. At a glance, implementing this recommendation is estimated to reduce the daily energy consumption by 75%. Currently the system constantly operates in the active mode and continuously samples data and transmit every two minutes. This is an estimated energy consumption of about 16 watt-hours/per day. About 69% of this energy is consumed by the PMS7003 particle sensor while the MICS-6814 multi-gas sensor, EFR32MG12 SoC and the BM280 sensors account for 28%, 1.5% and 1% of the energy consumption respectively. A breakdown of the system energy consumption analysis and the basis of my energy efficiency recommendation can be found in Appendix 3.

State representation of energy efficiency recommendation

To implement the above recommendation, a simple state representation is given below in Figure 4.6.



- 10 – Sensor Node off
- 20 – Gas sensor on (Pre-heating starts)
- 30 – Other sensors are turned on
- 40 – Data sampling
- 50 – All sensors off, Idle mode
- t1 – $T > 30\text{mins}$
- t2 – $T = 2\text{mins}$
- t3 – $T \geq 30\text{mins}$

Figure 4.16 State representation of energy efficiency recommendation

Figure 4.16 above depicts the recommended power transition for the sensor node. State 10 is the initial off state of the node. Sensor node is manually turned on in order to transition into state 20. The microcontroller unit resumes active state and Gas sensor preheating starts in state 20. A thirty minutes timer t1 starts in state 20. The expiration of this timer t1 transitions the system into state 30 where all other sensors are turned on. A new timer t2 starts a two minutes countdown allowing the sensors to stabilize. Once t2 elapses, the system changes to stage 40 where data sampling and transmission takes place for two-three minutes. On completion of data sampling and transmission, the system moves to state 50 where all sensors are turned off and the system resumes idle state. The system remains in an idle state for thirty minutes before returning back to state 20.

5. SUMMARY

5.1 Conclusion

Aimed at providing a low-cost environmental monitoring system that can be deployed in large numbers across a City like Tallinn, this thesis presents a cost-effective city environmental monitoring solution. This industry initiative based on Tallinn City need was developed in collaboration with Thinnect OU.

The objectives of this thesis aimed at improving the existing environmental monitoring sensor node were fulfilled.

The multi-gas sensor calibration was carried out and parameters such as base sensing resistance (R_0), relationship between the ADC value and Resistance, the relationship between sensing resistance ratio (R_s/R_0) and gas concentration in PPM were all determined. These parameters were also implemented in a C-program to ensure that the data acquisition and real-time conversion to standard engineering unit is done.

The analysis and data obtained from the existing sensor nodes were validated. The results presented in this thesis shows that the PMS7003 particulate matter sensor and the MICS-6814 multi-gas sensor used in this system need to be further investigated to improve their overall accuracy.

The BM280 Temperature, Humidity and Pressure sensor readings were validated and acceptable. The results show that the BM280 Temperature, Humidity and Pressure sensor has a percentage error of 21% and 15% in the measurements of temperature and relative humidity respectively. This error can be attributed to the difference in measurement location. The data used for validation is an average of these conditions for the whole of Tallinn and not for the exact location which our sensor node was deployed. The variation was anticipated and therefore acceptable for this study.

As regards the PMS7003 particulate matter sensor, only the PM10 data were validated against the conventional station at Liivalaia. The reason is that the conventional station at Liivalaia doesn't monitor other particulate matter sizes. The validated PM10 data show good correlation with the validating station but occasionally gave some questionable data. For example, there were few sudden

spikes recorded in the particulate matter readings and became low the next few minutes. Just as every system requires continuous improvement, this is one key areas of this system that needs to be further investigated.

The data captured by the MICS-6814 multi gas sensor was also analyzed and compared with the conventional station. To achieve this, the constants and equations derived during the calibration of this gas sensor were applied to the existing data obtained from the sensor node. This allowed me to covert the data to the standard engineering units in which our gases of interest are measured. After carefully analyzing the data from the different two different Thinnect sensor nodes used in data capturing, it was realized that by compensating for the error in the readings of the MICS-6814 multi-gas sensor, it can reliably measure the carbon monoxide level with less than 15% percentage error. This compensation includes reducing the calibration constants used in the data conversion as shown in Figure 4.12 above. On the other hand, the nitrogen dioxide measurements obtained from the MICS-6814 multi-gas sensor were discovered to have huge discrepancies in thousands when compared to the readings from the conventional station. Further steps were taken to deploy a standalone gas sensor node designed and calibrated by a different manufacture to capture similar data. The result from this new sensor node was also found to have huge discrepancies in thousands. This raised a question of whether the validating station is reporting the nitrogen dioxide data in the right engineering unit or the portable multi-gas sensors deployed are ineffective in the measuring nitrogen dioxide. Further investigation is recommended to be carried out to ascertain why the difference between the two portable sensor nodes (Thinnect and the standalone node) and the conventional environmental monitoring station is in the range of thousands.

In conclusion, the current power consumption of the system was analyzed, and an energy efficiency strategy was recommended for the system. The recommended strategy if implemented, is estimated to improve the energy efficiency of the system by 75%.

5.2 Kokkuvõte eesti keeles

Magistritöö käsitleb kuluefektiivse linnakeskkonna jälgimise lahendust, mille eesmärgiks on madala hinnaga keskkonnaparameetrite jälgimise seadme loomine, mida on võimalik paigaldada suurtes kogustes erinevates linnades, näiteks Tallinnas. Antud praktiline töö viidi läbi koostöös ettevõttega Thinnect. Töö käigus saavutati selle eesmärk, milleks oli olemasoleva keskkonna jälgimise sensorilahenduse täiendamine.

Töö käigus viidi läbi mitmete gaaside mõõtmiseks sobiliku sensori kalibreerimine ning tehti kindlaks parameetrid, nagu sensori baastakistus (R_0), seos analoog-digitaal muunduri väljundi ning takistuse vahel, seos sensori takistuse suhte (R_s/R_0) ja gaaside kontsentratsiooni (mida mõõdetakse ühikuga ppm) vahel. Mõõdetavate suuruste arvutamiseks realiseeriti rakendus C-keeles, tagamaks andmehõive ja andmete konverteerimine mõõdetavateks suurusteks.

Töö käigus valideeriti tehtud analüüsi ja olemasolevate sensorite poolt kogutud ja andmeid. Magistritöös toodud tulemused näitavad, et PMS7003 osakeste sensor ja mitmete gaaside mõõtmiseks sobilik sensor MICS-6814 vajavad edasisi uuringuid nende täpsuse parandamiseks.

BM280 temperatuuri, õhuniiskuse ja õhurõhu sensori lugemeid valideeriti ning leiti, et need on aktsepteeritavad. Tulemused näitavad, et BM280 temperatuuri, õhuniiskuse ja õhurõhu sensori viga on 21% temperatuuri mõõtmisel ja 15% õhuniiskuse mõõtmisel. Selle vea põhjuseks võib olla mõõtmiskoha erinevus. Andmed, mida kasutati nende sensorite lugemite valideerimiseks, kehtisid kogu Tallinna kohta ja mitte selle koha kohta, kus sensorid paiknesid. Erinevus oli oodatav ja seega antud töö kontsektis aktsepteeritav.

PMS7003 osakeste sensori puhul valideeriti ainult PM10 (10 mikromeetri suuruste osakeste kontsentratsioon) andmeid Liivalaia tänaval paikneva olemasoleva Eesti Keskkonnauuringute Keskuse sensorjaama andmete vastu. PM10 parameetri valiku põhjuseks on fakt, et Liivalaia tänav sensorjaam suudab mõõta ainult antud suurusega osakeste kontsentratsiooni. PM10 sensori andmete valideerimise tulemused olid positiivsed, kuid vahel andis sensor juhuslikke küsitava väärtusega lugemeid. Näiteks olid 64 juhtu, kui sensor andis normaalsest kõrgemaid lugemeid ning taastus esialgsele tasemele järgmise mõne minuti jooksul. Nagu ka iga süsteemi puhul, mis vajab pidevat täiendamist, on see üks võtmeküsimusi, mis

vajab antud süsteemi puhul täiendavaid uuringuid.

Magistritöö raames uuriti ka MICS-6814 mitmete gaaside mõõtmiseks sobiliku sensori tööd ja võrreldi selle sensori lugemeid olemasoleva sensorjaama lugemitega. Selle saavutamiseks rakendati sensori kalibreerimisel leitud konstante ja valemeid juba kogutud sensorandmetele. See võimaldas teisendada juba kogutud andmed gaaside mõõtesuurusteks. Analüüsides andmeid, mis olid kogutud kahe erineva Thinnecti sensori poolt, jõuti järeldusele, et kompenseerides MICS-6814 gaasisensori viga, on see võimeline mõõtma CO taset vähem kui 15% veaga. Kompenseerimiseks on vaja vähendada kalibratsioonikoefitsendi suurust nagu on näidatud töös joonisel 28. Kahjuks olid lämmastikdioksiidi lugemite erinevus olemasoleva mõõtejaama ning MICS-6814 sensori lugemite vahel tuhandetes. Lisaks Thinnecti sensorite lugemite analüüsile rakendati töös ka autonoomset tootja poolt kalibreeritud gaaside sensorit. Ka antud sensori lämmastikdioksiidi lugemite erinevus oli tuhandetes. See tõstatab küsimuse, kas olemasoleva Eesti Keskkonnauuringute Keskuse sensorjaama poolt raporteeritav lämmastikdioksiidi kontsentratsiooni lugemeid raporteeritakse õigesti ühikutes või kas töös kasutatud sensorid ei ole võimelised korrektselt mõõtma lämmastikdioksiidi kontsentratsiooni. Selles suunas on vajalikud lisauuringud tegemaks kindlaks millest tuleb erinevus erinevate sensorite sensorlugemites.

Magistritöös analüüsiti ka süsteemi energiatarvet ja tehti soovitused süsteemi energiatarbe vähendamiseks. Kui tehtud soovitusi rakendatakse, on võimalik süsteemi energiatarbe vähendamine 75%.

5.3 Future Work

The research work in this thesis can be further improved by looking into the accuracy challenges of some of the sensors used in this project. Concerning the multi gas sensor, the huge measurement discrepancies in the nitrogen dioxide readings should be investigated to ascertain if the problem is from the gas sensors or the station used for validation. Furthermore, in order to increase the accuracy of the carbon monoxide reading, a software compensation could be implemented to compensate for impacts of environmental conditions such as ambient temperature, relative humidity, and pressure. The particulate matter sensor also needs to be further investigated, in order to find out the root cause of the sudden spikes highlighted in Chapter 4.

Conclusively, the energy efficiency recommendation in section 4.4 should be considered.

LIST OF REFERENCES

- [1] Health Effects Institute, "Traffic-Related Air Pollution: A Critical Review of the Literature on Emissions, Exposure, and Health Effects | Health Effects Institute," *A Spec. Rep. Institute's Panel Heal. Eff. Traffic-Related Air Pollut.*, vol. Report 17, 2010.
- [2] "WHO | Ambient air pollution: A global assessment of exposure and burden of disease," *WHO*, 2016.
- [3] F. Gozzi, G. Della Ventura, and A. Marcelli, "Mobile monitoring of particulate matter: State of art and perspectives," *Atmospheric Pollution Research*, vol. 7, no. 2. Elsevier B.V., pp. 228–234, 2016.
- [4] B. Fubini and I. Fenoglio, "Toxic potential of mineral dusts," *Elements*, vol. 3, no. 6, pp. 407–414, Dec. 2007.
- [5] R. McConnell *et al.*, "Childhood incident asthma and traffic-related air pollution at home and school," *Environ. Health Perspect.*, vol. 118, no. 7, pp. 1021–1026, 2010.
- [6] A. Abelsohn, M. D. Sanborn, B. J. Jessiman, and E. Weir, "Identifying and managing adverse environmental health effects: 6. Carbon monoxide poisoning," *CMAJ*, vol. 166, no. 13. Canadian Medical Association, pp. 1685–1690, 2002.
- [7] D. Campbell-Lendrum and C. Corvalán, "Climate change and developing-country cities: Implications for environmental health and equity," *Journal of Urban Health*, vol. 84, no. SUPPL. 1. Springer, p. 109, May-2007.
- [8] D. Smith, P. Španěl, J. Herbig, and J. Beauchamp, "Mass spectrometry for real-time quantitative breath analysis," *J. Breath Res.*, vol. 8, no. 2, p. 027101, Mar. 2014.
- [9] European Environmental Agency, *Air quality in Europe – 2019 report – EEA Report No 10/2019*, no. 10. 2019.
- [10] W. H. Organization, "Review of evidence on health aspects of air pollution–REVIHAAP Project," 2017.
- [11] A. Kadri, E. Yaacoub, M. Mushtaha, and A. Abu-Dayya, "Wireless sensor network for real-time air pollution monitoring," in *2013 1st International Conference on Communications, Signal Processing and Their Applications, ICCSPA 2013*, 2013.
- [12] "Air quality standards under the Air Quality Directive, and WHO air quality guidelines — European Environment Agency." [Online]. Available: <https://www.eea.europa.eu/themes/data-and-maps/figures/air-quality-standards-under-the>. [Accessed: 24-Feb-2020].

- [13] P. S. Kanaroglou *et al.*, "Establishing an air pollution monitoring network for intra-urban population exposure assessment: A location-allocation approach," in *Atmospheric Environment*, 2005, vol. 39, no. 13, pp. 2399–2409.
- [14] M. Jerrett, M. Buzzelli, R. T. Burnett, and P. F. DeLuca, "Particulate air pollution, social confounders, and mortality in small areas of an industrial city," in *Social Science and Medicine*, 2005, vol. 60, no. 12, pp. 2845–2863.
- [15] D. Hasenfratz, O. Saukh, C. Walser, C. Hueglin, M. Fierz, and L. Thiele, "Pushing the spatio-temporal resolution limit of urban air pollution maps," in *2014 IEEE International Conference on Pervasive Computing and Communications, PerCom 2014*, 2014, pp. 69–77.
- [16] J. Ikram, A. Tahir, H. Kazmi, Z. Khan, R. Javed, and U. Masood, "View: implementing low cost air quality monitoring solution for urban areas," *Environ. Syst. Res.*, vol. 1, no. 1, p. 10, Oct. 2012.
- [17] S. Choi, N. Kim, H. Cha, and R. Ha, "Micro sensor node for air pollutant monitoring: Hardware and software issues," *Sensors*, vol. 9, no. 10, pp. 7970–7987, Oct. 2009.
- [18] B. Ostro, J. M. Sanchez, C. Aranda, and G. S. Eskeland, "Air pollution and mortality: Results from a study of Santiago, Chile," *J. Expo. Anal. Environ. Epidemiol.*, vol. 6, no. 1, pp. 97–114, Jan. 1996.
- [19] D. Gillis, I. Semanjski, and D. Lauwers, "How to monitor sustainable mobility in cities? Literature review in the frame of creating a set of sustainable mobility indicators," *Sustainability (Switzerland)*, vol. 8, no. 1. MDPI AG, pp. 1–30, 2016.
- [20] I. Semanjski, A. J. L. Aguirre, J. De Mol, and S. Gautama, "Policy 2.0 platform for mobile sensing and incentivized targeted shifts in mobility behavior," *Sensors (Switzerland)*, vol. 16, no. 7, Jul. 2016.
- [21] I. Semanjski, R. Bellens, S. Gautama, and F. Witlox, "Integrating big data into a sustainable mobility policy 2.0 planning support system," *Sustain.*, vol. 8, no. 11, Nov. 2016.
- [22] B. S. Beckerman *et al.*, "The association between chronic exposure to traffic-related air pollution and ischemic heart disease," *J. Toxicol. Environ. Heal. - Part A Curr. Issues*, vol. 75, no. 7, pp. 402–411, Apr. 2012.
- [23] M. Brauer, C. Lencar, L. Tamburic, M. Koehoorn, P. Demers, and C. Karr, "A cohort study of traffic-related air pollution impacts on birth outcomes," *Environ. Health Perspect.*, vol. 116, no. 5, pp. 680–686, May 2008.
- [24] K. A. Miller *et al.*, "Long-term exposure to air pollution and incidence of cardiovascular events in women," *N. Engl. J. Med.*, vol. 356, no. 5, pp. 447–458, Feb. 2007.

- [25] B. Ritz, M. Wilhelm, and Y. Zhao, "Air pollution and infant death in Southern California, 1989-2000," *Pediatrics*, vol. 118, no. 2, pp. 493–502, Aug. 2006.
- [26] M. Johnson, V. Isakov, J. S. Touma, S. Mukerjee, and H. Özkaynak, "Evaluation of land-use regression models used to predict air quality concentrations in an urban area," *Atmos. Environ.*, vol. 44, no. 30, pp. 3660–3668, Sep. 2010.
- [27] R. Beelen, G. Hoek, P. Fischer, P. A. van den Brandt, and B. Brunekreef, "Estimated long-term outdoor air pollution concentrations in a cohort study," *Atmos. Environ.*, vol. 41, no. 7, pp. 1343–1358, 2007.
- [28] B. Brunekreef *et al.*, "Effects of long-term exposure to traffic-related air pollution on respiratory and cardiovascular mortality in the Netherlands: the NLCS-AIR study," *Res. Rep. Health. Eff. Inst.*, no. 139, 2009.
- [29] P. Kumar *et al.*, "The rise of low-cost sensing for managing air pollution in cities," *Environment International*, vol. 75. Elsevier Ltd, pp. 199–205, 01-Feb-2015.
- [30] W. J. Farrell, S. Weichenthal, M. Goldberg, and M. Hatzopoulou, "Evaluating air pollution exposures across cycling infrastructure types: Implications for facility design," *J. Transp. Land Use*, vol. 8, no. 3, pp. 131–149, May 2015.
- [31] R. M. White, I. Paprotny, F. Doering, W. E. Cascio, P. A. Solomon, and L. A. Gundel, "Sensors and 'apps' for community-based: Atmospheric monitoring," *EM Air Waste Manag. Assoc. Mag. Environ. Manag.*, no. MAY, pp. 36–40, May 2012.
- [32] E. G. Snyder *et al.*, "The changing paradigm of air pollution monitoring," *Environ. Sci. Technol.*, vol. 47, no. 20, pp. 11369–11377, Oct. 2013.
- [33] European Commission's Joint Research Centre, "Measuring air pollution with low-cost sensors Thoughts on the quality of data measured by sensors."
- [34] M. Alexandre and M. Gerboles, "Review of Small Commercial Sensors for Indicative Monitoring of Ambient Gas," 2012, vol. 30.
- [35] O. of R. & Development, "Air Sensor Guidebook."
- [36] J. Chou, "Gas Sensor Calibration definition," *Hazard. Gas Monit. A Pract. Guid. to Sel. Oper. Appl.*, pp. 161–173, 1999.
- [37] "Particulate Matter in the United Kingdom Summary," 2005.
- [38] B. D. Grover, "Measurement of total PM_{2.5} mass (nonvolatile plus semivolatile) with the Filter Dynamic Measurement System tapered element oscillating microbalance monitor," *J. Geophys. Res.*, vol. 110, no. D7, p. D07S03, Apr. 2005.
- [39] W. Yi, K. Lo, T. Mak, K. Leung, Y. Leung, and M. Meng, "A Survey of Wireless Sensor Network Based Air Pollution Monitoring Systems," *Sensors*, vol. 15,

- no. 12, pp. 31392–31427, Dec. 2015.
- [40] D. Hasenfratz *et al.*, "Deriving high-resolution urban air pollution maps using mobile sensor nodes," in *Pervasive and Mobile Computing*, 2015, vol. 16, no. PB, pp. 268–285.
- [41] D. Hasenfratz, O. Saukh, S. Sturzenegger, and L. Thiele, *Participatory Air Pollution Monitoring Using Smartphones*. 2012.
- [42] P. Dutta and D. Culler, "Mobility Changes Everything in Low-Power Wireless Sensor networks."
- [43] M. Budde, L. Zhang, and M. Beigl, "Distributed, Low-cost Particulate Matter Sensing: Scenarios, Challenges, Approaches," 2014.
- [44] M. Budde, M. Busse, and M. Beigl, "Investigating the use of commodity dust sensors for the embedded measurement of particulate matter," in *9th International Conference on Networked Sensing Systems, INSS 2012 - Conference Proceedings*, 2012.
- [45] M. Budde, R. El Masri, T. Riedel, and M. Beigl, "Enabling low-cost particulate matter measurement for participatory sensing scenarios," in *Proceedings of the 12th International Conference on Mobile and Ubiquitous Multimedia, MUM 2013*, 2013, pp. 1–10.
- [46] M. I. Khadem and V. Sgârciu, "Smart sensor nodes for airborne particulate concentration detection," *UPB Sci. Bull. Ser. C Electr. Eng. Comput. Sci.*, vol. 76, no. 4, pp. 3–12, 2014.
- [47] L. Li, Y. Zheng, and L. Zhang, "Demonstration abstract: PiMi air box - A cost-effective sensor for participatory indoor quality monitoring," in *IPSN 2014 - Proceedings of the 13th International Symposium on Information Processing in Sensor Networks (Part of CPS Week)*, 2014, pp. 327–328.
- [48] B. Rashid and M. H. Rehmani, "Applications of wireless sensor networks for urban areas: A survey," *Journal of Network and Computer Applications*, vol. 60. Academic Press, pp. 192–219, 01-Jan-2016.
- [49] J. Hendee *et al.*, "Wireless architectures for coral reef environmental monitoring," 2012.
- [50] C. Albaladejo, P. Sánchez, A. Iborra, F. Soto, J. A. López, and R. Torres, "Wireless Sensor Networks for Oceanographic Monitoring: A Systematic Review," *Sensors*, vol. 10, no. 7, pp. 6948–6968, Jul. 2010.
- [51] J. Lloret, M. Garcia, D. Bri, and S. Sendra, "A Wireless Sensor Network Deployment for Rural and Forest Fire Detection and Verification," *Sensors*, vol. 9, no. 11, pp. 8722–8747, Oct. 2009.
- [52] I. F. Akyildiz, W. Su, Y. Sankarasubramaniam, and E. Cayirci, "Wireless sensor networks: A survey," *Comput. Networks*, vol. 38, no. 4, pp. 393–422,

- Mar. 2002.
- [53] J. Yick, B. Mukherjee, and D. Ghosal, "Wireless sensor network survey," *Comput. Networks*, vol. 52, no. 12, pp. 2292–2330, Aug. 2008.
 - [54] A. C. Lim, A. Goossens, A. C. J. Ravelli, K. Boer, H. W. Bruinse, and B. W. J. Mol, "Utilizing new evidence in the prevention of recurrent preterm birth," *J. Matern. Neonatal Med.*, vol. 24, no. 12, pp. 1456–1460, Dec. 2011.
 - [55] C. H. See, K. V. Horoshenkov, R. A. Abd-Alhameed, Y. F. Hu, and S. J. Tait, "A low power wireless sensor network for gully pot monitoring in urban catchments," *IEEE Sens. J.*, vol. 12, no. 5, pp. 1545–1553, 2012.
 - [56] V. Hejlová and V. Voženílek, "Wireless Sensor Network Components for Air Pollution Monitoring in the Urban Environment: Criteria and Analysis for Their Selection," *Wirel. Sens. Netw.*, vol. 05, no. 12, pp. 229–240, 2013.
 - [57] C. Antonopoulos, F. Kerasiotis, C. Koulamas, G. Papadopoulos, and S. Koubias, "Experimental evaluation of the waspmote platform power consumption targeting ambient sensing," in *Proceedings - 2015 4th Mediterranean Conference on Embedded Computing, MECO 2015 - Including ECyPS 2015, BioEMIS 2015, BioICT 2015, MECO-Student Challenge 2015*, 2015, pp. 124–128.
 - [58] "Waspote Plug & Sense! Technical Guide."
 - [59] W. Fuertes *et al.*, "Distributed system as internet of things for a new low-cost, air pollution wireless monitoring on real time," in *Proceedings - 2015 IEEE/ACM 19th International Symposium on Distributed Simulation and Real Time Applications, DS-RT 2015*, 2016, pp. 58–67.
 - [60] Y. Ma, M. Richards, M. Ghanem, Y. Guo, and J. Hassard, "Air Pollution Monitoring and Mining Based on Sensor Grid in London," *Sensors*, vol. 8, no. 6, pp. 3601–3623, Jun. 2008.
 - [61] Y. J. Jung *et al.*, "Design of Sensor Data Processing Steps in an Air Pollution Monitoring System," *Sensors*, vol. 11, no. 12, pp. 11235–11250, Nov. 2011.
 - [62] A. Bagula, M. Zennaro, G. Inggs, S. Scott, and D. Gascon, "Ubiquitous Sensor Networking for Development (USN4D): An Application to Pollution Monitoring," *Sensors*, vol. 12, no. 1, pp. 391–414, Jan. 2012.
 - [63] "EFR32xG21 Wireless Gecko Reference Manual."
 - [64] "Digital universal particle concentration sensor PMS7003 series data manual," 2016.
 - [65] "SMENETE – Next Generation Networking." [Online]. Available: <https://www.thinnect.com/technology/smenete-next-generation/>. [Accessed: 22-May-2020].
 - [66] "The MiCS-6814 is a compact MOS sensor with three fully independent

sensing elements on one package. Features Detectable gases.”

[67] “BME280-Data sheet,” 2018.

[68] Thinnect, “Smart City Gateway Datasheet,” p. 94085.

[69] “Weather in April 2020 in Tallinn, Estonia.” [Online]. Available:
<https://www.timeanddate.com/weather/estonia/tallinn/historic?month=4&year=2020>. [Accessed: 19-May-2020].

[70] [Http://ohuseire.ee/en](http://ohuseire.ee/en), “Air Quality Management System.” [Online]. Available:
<http://ohuseire.ee/en>. [Accessed: 13-May-2020].

APPENDIX 1 Plots showing sensor data obtained on 30-04-2020 from the Thinnect node located at Rahu, Tallinn

This section contains the result of the data obtained for the Thinnect sensor node deployed at Rahu station on 30-April-2020 in comparison with the data from the conventional environmental monitoring station located in Rahu, Tallinn, for the same period.

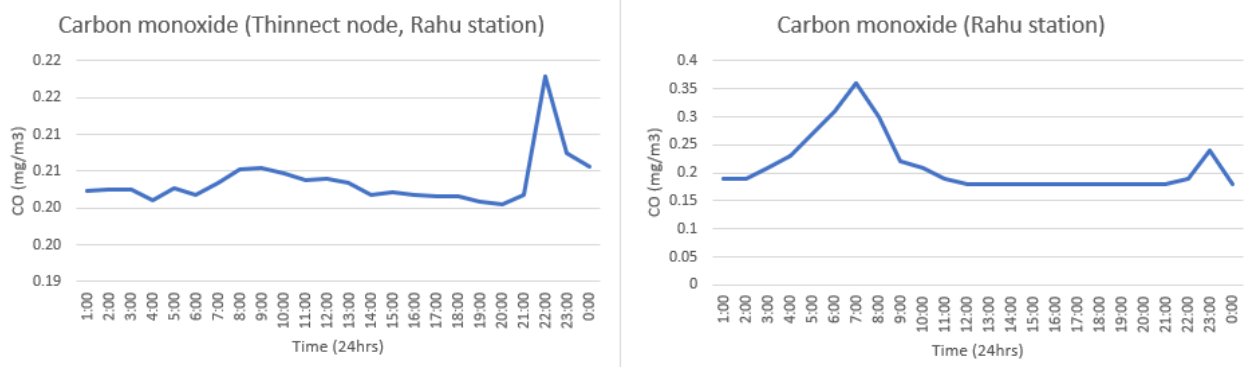


Figure A1.1 A side-by-side comparison of charts showing carbon monoxide level on 30-April-2020 obtained from the Thinnect sensor node (using the experimental calibration constant, $R_0=12.5k\Omega$) versus the conventional air monitoring station (right chart) located in Rahu, Tallinn.

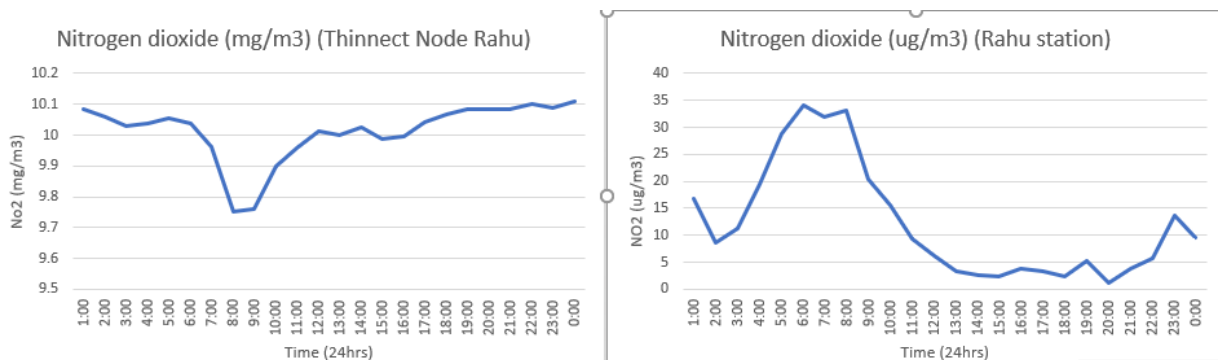


Figure A1.2 A side-by-side comparison of charts showing nitrogen dioxide level on 30-April-2020 obtained from the Thinnect sensor node (in mg/m3) versus the conventional air monitoring station (in $\mu\text{g}/\text{m}^3$) located in Rahu, Tallinn.

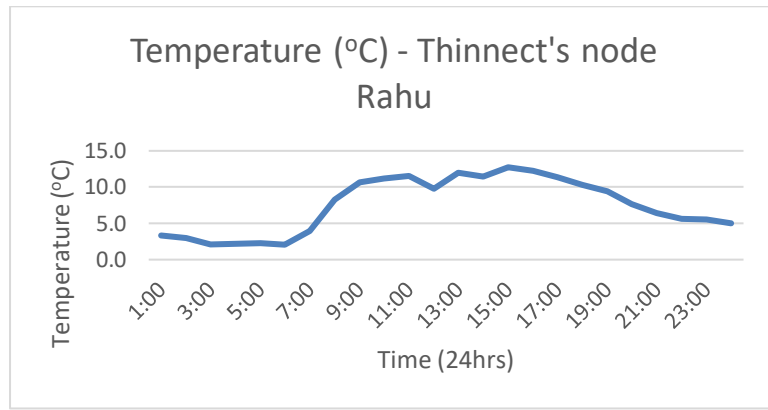


Figure A1.3 A plot showing the temperature reading on 30-April-2020 obtained from the Thinnect sensor node located in Rahu, Tallinn

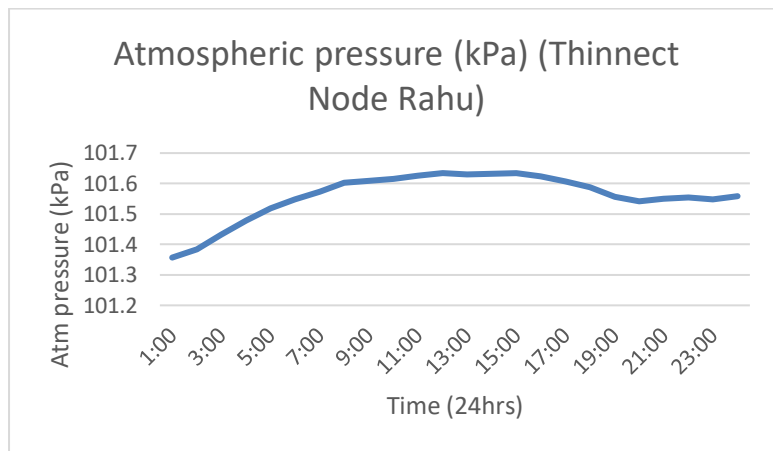


Figure A1.4 A plot showing the atmospheric pressure reading on 30-April-2020 obtained from the Thinnect sensor node located in Rahu, Tallinn

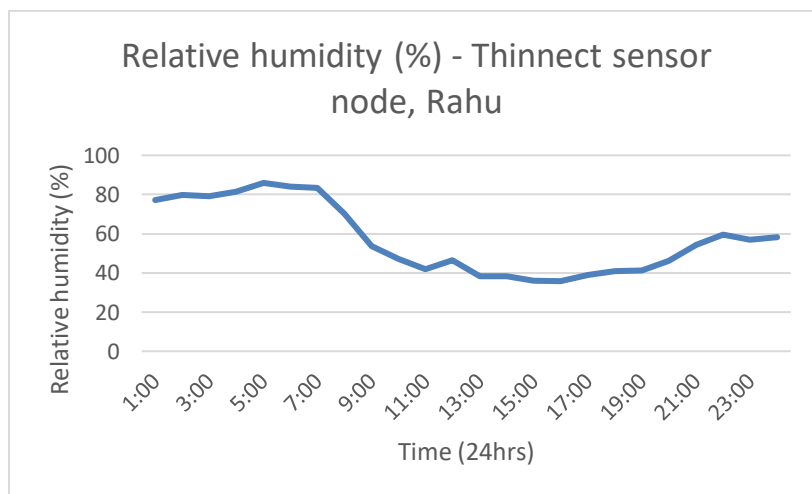


Figure A1.5 A plot showing the relative humidity reading on 30-April-2020 obtained from the Thinnect sensor node located in Rahu, Tallinn

APPENDIX 2 Firmware code for the multi gas sensor

This section contains the firmware code to convert the Multi gas sensor analog signal to gas concentration in PPM.

Header file

```
1. /*MiCS-6184 Conversion : ADC to Engineering Values
2. *
3. * main.h
4. */
5.
6.
7. #define NH3_SENSOR 0
8. #define CO_SENSOR 1
9. #define NO2_SENSOR 2
10.
11. #define NH3 0
12. #define CO 1
13. #define NO2 2
14.
15. // Base resistance (R0) Value in k
16. #define R0_NH3 69.9
17. #define R0_CO 88.66
18. #define R0_NO2 6.2
19.
20. /* return the resistance value for the current ADC value for sensor*/
21. float getSensorRs(unsigned char gasCh);
22.
23. /* calculate the current PPM for a specific gas */
24. float calcGas(int gas);
25.
```

*Main C *

```
1. /* MiCS-6184 MiCS-6184 Conversion : ADC to Engineering Values
2. *
3. */
4.
5. #include "main.h"
6. /*****
7. *****/
8. ** Function name: getSensorRs
9. ** Descriptions: Converts ADC value to current sensor resistance
10. **
11. ** @param gasCh : ID of gas to get
12. **
13. ** return code
14. ** 0 = Error
15. **
16. *****/
17. //get current sensor resistance
18. float getSensorRs(unsigned char gasCh)
19. {
20.     int a = 0;
21.     //first get sensor resistance ADC value
```

```

21.     switch(gasCh)
22.     {
23.         case NH3_SENSOR:           // NH3
24.             a = getAdcValue(VALUE_NH3); //getAdcValue returns current ADC value of
gas
25.             break;
26.
27.         case CO_SENSOR:           // CO
28.             a = getAdcValue(VALUE_CO);
29.             break;
30.
31.         case NO2_SENSOR:          // NO2
32.             a = getAdcValue(VALUE_NO2);
33.             break;
34.
35.         default;;
36.     }
37.
38. /* then calculate the resistance value using derived equation 4.3 in section 4.
1.1,
39.
40.  $R_s = (56k * ADC\_Current\_Reading) / (ADC\_Max\_Reading - ADC\_Current\_Reading)$ 
41. Where;
42. Rs= Sensor resistance
43.
44. */
45.     float r = 56.0*(float)a/(1023.0-(float)a);
46.
47.     return r;
48. }
49.
50.
51.
52. /*****
*****
53. ** Function name:           calcGas
54. ** Description:           calculates gas concentration of CO, NH3 and NO2
55. **                         See Chapter 4 for calculation basis
56. ** Parameters:
57. **                         gas - gas name CO or NO2 or NH3
58. ** Returns:
59. **                         float - gas concentration in PPM
60. **
61. **
62. **
63. *****/
64. float calcGas(int gasName)
65. {
66.
67.     float Rs_NH3, Rs_CO, Rs_NO2;
68.     float ratio_NH3, ratio_CO, ratio_NO2;
69.
70.
71.
72.
73.     // get sensor current resistance (Rs) value
74.     Rs_NH3 = getSensorRs(NH3_SENSOR);
75.     Rs_CO = getSensorRs(CO_SENSOR);
76.     Rs_NO2 = getSensorRs(NO2_SENSOR);
77.
78.     //calculate resistance ratio (Rs/Ro)
79.     ratio_NH3 = Rs_NH3/R0_NH3;
80.     ratio_CO = Rs_CO/R0_CO;
81.     ratio_NO2 = Rs_NO2/R0_NO2;
82.

```

```

83.
84.     float c = 0;
85.
86.     switch(gasName)
87.     {
88.         case CO: // Calculate Carbon Monoxide from equation 4.4, and check i
f result is within limits
89.
90.             c = pow(ratio_CO, -1.182)*4.4922;
91.             if (c < 0.1 || c > 1000) {
92.                 c=0;
93.             }
94.             break;
95.     }
96.     case NO2: // Calculate Nitrogen Dioxide from equation 4.5, and check
if result is within limits
97.     {
98.
99.         c = (ratio_NO2 * 0.1499) + 0.0042;
100.        if (c < 0.01 || c > 7) {
101.            c=0;
102.        }
103.        break;
104.    }
105.    case NH3: // Calculate Ammonia from equation 4.6, and check i
f result is within limits
106.    {
107.
108.        c = pow(ratio_NH3, -1.918)*0.5908;
109.        if (c < 1 || c > 160) {
110.            c=0;
111.        }
112.        break;
113.    }
114.    default:
115.        break;
116.    }
117.
118.    //verify result is floating point and return
119.    return isnan(c)?-1:c;
120. }
121.

```

APPENDIX 3 The sensor node energy consumption and efficiency analysis

The table below shows the energy consumption analysis of the sensor node. Two scenarios were considered. The first scenario is the current state of the system where the sensor node acquires and transmits data every two mins. The other scenario is the estimated energy consumption if the sensor node is configured to acquire and transmit data every one-hour. A total energy reduction of about 76% was estimated to be saved if the latter option is adopted.

Table A3.1 The sensor node energy consumption and efficiency analysis.

Sensor	Active current (mA)	Standby current (uA)	Voltage (V)	Active Power consumption (mW)	Standby Power consumption (mW)	24h energy consumption if operating actively 35mins in every hour (only for gas sensor & MCU) (watt-hour)	24h energy consumption if operating in active mode 5mins in every hour (watt-hour)	24h energy consumption if operating in standby mode for 55 mins in every hour (watt-hour)	Total energy consumption in 24 hours if sensor node runs once every hour (watt-hours/day)	Total energy consumption in 24 hours if sensor node runs constantly in 24hrs (watt-hours/day)	Energy savings (%)
PMS7003 - Particle sensor	100	200	5	500	1		1	0.022	1.022	11	91
BME280 - Temperature, Pressure & Humidity sensor	0.633	0.3	3.3	2.1	0.001		0.0042	0.000022	0.004	0.101	96
MICS-6814 - Multi-gas sensor (heater)			5	185		2.59			2.590	4.440	42
MICS-6814 - Multi-gas sensor (sensing layer)			5	8		0.112			0.112	0.192	42
EFR32MG SoC	2.8	0.24	3.3	9.24	0.000792	0.12936		0.000008	0.129	0.222	42
	assuming 40MHz @ 70uA/mHz	assuming 5MHz @ 47uA/mHz						24hrs consumption if MCU Operates standby 25 mins every hour			
Total consumption				695.09					3.86	15.95	76

APPENDIX 4 Pictures showing the Thinnect sensor node for environmental monitoring

More pictures of the Thinnect sensor node.



Figure A4.1 Top compartment of the sensor node

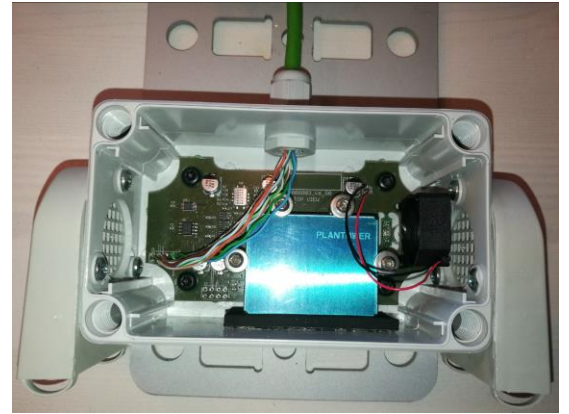


Figure 4.3 Lower compartment of sensor node



Figure A4.2 Complete sensor node